J|A|C|S
ARTICLES
Published on Web 08/16/2002

# Ab Initio Studies on $Al^+(H_2O)_n$, $HAlOH^+(H_2O)_{n-1}$, and the Size-Dependent $H_2$ Elimination Reaction

Chi-Kit Siu,[†] Zhi-Feng Liu,*[,†] and John S. Tse[‡]

*Contribution from the Department of Chemistry, The Chinese University of Hong Kong, Shatin, Hong Kong, China, and Steacie Institute for Molecular Sciences, National Research Council of Canada, Ottawa, Ontario K1A 0R6, Canada*

Received July 19, 2001

**Ⓦ This paper contains enhanced objects available on the Internet at http://pubs.acs.org/journals/jacsat.**

***Abstract:*** We report computational studies on $Al^+(H_2O)_n$, $n = 6-9$, and $HAlOH^+(H_2O)_{n-1}$, $n = 6-14$, by the density functional theory based ab initio molecular dynamics method, employing a planewave basis set with pseudopotentials, and also by conventional methods with Gaussian basis sets. The mechanism for the intracluster $H_2$ elimination reaction is explored. First, a new size-dependent insertion reaction for the transformation of $Al^+(H_2O)_n$ into $HAlOH^+(H_2O)_{n-1}$ is discovered for $n \geq 8$. This is because of the presence of a fairly stable six-water-ring structure in $Al^+(H_2O)_n$ with 12 members, including the $Al^+$. This structure promotes acidic dissociation and, for $n \geq 8$, leads to the insertion reaction. Gaussian based BPW91 and MP2 calculations with 6-31G* and 6-31G** basis sets confirmed the existence of such structures and located the transition structures for the insertion reaction. The calculated transition barrier is 10.0 kcal/mol for $n = 9$ and 7.1 kcal/mol for $n = 8$ at the MP2/6-31G** level, with zero-point energy corrections. Second, the experimentally observed size-dependent $H_2$ elimination reaction is related to the conformation of $HAlOH^+(H_2O)_{n-1}$, instead of $Al^+(H_2O)_n$. As $n$ increases from 6 to 14, the structure of the $HAlOH^+(H_2O)_{n-1}$ cluster changes into a caged structure, with the Al−H bond buried inside, and protons produced in acidic dissociation could then travel through the $H_2O$ network to the vicinity of the Al−H bond and react with the hydride H to produce $H_2$. The structural transformation is completed at $n = 13$, coincident approximately with the onset of the $H_2$ elimination reaction. From constrained ab initio MD simulations, we estimated the free energy barrier for the $H_2$ elimination reaction to be 0.7 eV (16 kcal/mol) at $n = 13$, 1.5 eV (35 kcal/mol) at $n = 12$, and 4.5 eV (100 kcal/mol) at $n = 8$. The existence of transition structures for the $H_2$ elimination has also been verified by ab initio calculations at the MP2/6-31G** level. Finally, the switch-off of the $H_2$ elimination for $n > 24$ is explored and attributed to the diffusion of protons through enlarged hydrogen bonded $H_2O$ networks, which reduces the probability of finding a proton near the Al−H bond.

## Introduction

The importance of solvated metal ion clusters is well known.[1−8] They are the models for the solvation of ions in liquid, the understanding of which is of fundamental importance not only for solution chemistry, but also for many biological systems. In recent years, the role of such clusters as an intermediate state between the gas and the solution phases has attracted much attention. The size-dependence effects, revealed by carefully controlling the number of solvent molecules in a cluster, provide invaluable insights into the solvation dynamics and its influence on chemical reactions. Many such systems have been studied over the years by both experiments[9−28] and

* To whom correspondence should be addressed. Fax: +852-2603-5057. E-mail: zfliu@cuhk.edu.hk. Phone: +852-2609-6358.
[†] The Chinese University of Hong Kong.
[‡] National Research Council of Canada.

(1) Lisy, J. M. *Int. Rev. Phys. Chem.* **1997**, *16*, 267.
(2) Castleman, A. W., Jr.; Bowen, K. H. *J. Phys. Chem.* **1996**, *100*, 12911.
(3) Fuke, K.; Hashimoto, K.; Iwata, S. *Adv. Chem. Phys.* **1999**, *110*, 431.
(4) Niedner-Schatteburg, G.; Bondybey, V. E. *Chem. Rev.* **2000**, *100*, 4059.
(5) Magnera, T. F.; David, D. E.; Michl, J. *J. Am. Chem. Soc.* **1989**, *111*, 4100.
(6) Magnera, T. F.; David, D. E.; Stulik, D.; Orth, R. G.; Jonkman, H. J.; Michl, J. *J. Am. Chem. Soc.* **1989**, *111*, 5036.
(7) Marinelli, P. J.; Squires, R. R. *J. Am. Chem. Soc.* **1989**, *111*, 4101.
(8) Jayaweera, P.; Blades, A. T.; Ikonomou, M. G.; Kebarle, P. *J. Am. Chem. Soc.* **1990**, *112*, 2452.
(9) Draves, J. A.; Lisy, J. M. *J. Am. Chem. Soc.* **1990**, *112*, 9006.
(10) Selegue, T. J.; Lisy, J. M. *J. Am. Chem. Soc.* **1994**, *116*, 4874.
(11) Weinheimer, C. J.; Lisy, J. M. *J. Chem. Phys.* **1996**, *105*, 2938.
(12) Weinheimer, C. J.; Lisy, J. M. *J. Phys. Chem.* **1996**, *100*, 15305.
(13) Zhang, X.; Castleman, A. W., Jr. *J. Am. Chem. Soc.* **1992**, *114*, 8607.
(14) Harms, A. C.; Khanna, S. N.; Chen, A. B.; Castleman, A. W., Jr. *J. Chem. Phys.* **1994**, *100*, 3540.
(15) Sanekata, M.; Misaizu, F.; Fuke, K.; Iwata, S.; Hashimoto, K. *J. Am. Chem. Soc.* **1995**, *117*, 747.
(16) Sanekata, M.; Misaizu, F.; Fuke, K. *J. Chem. Phys.* **1996**, *104*, 9768.
(17) Misaizu, F.; Sanekata, M.; Fuke, K.; Iwata, S. *J. Chem. Phys.* **1994**, *100*, 1161.
(18) Lu, W. Y.; Yang, S. H. *J. Phys. Chem. A* **1998**, *102*, 825.
(19) Barran, P. E.; Walker, N. R.; Stace, A. J. *J. Chem. Phys.* **2000**, *112*, 6173.
(20) Stace, A. J.; Dobson, M. P.; Woodward, C. A. *Chem. Phys. Lett.* **1997**, *267*, 171.


**10.1021/ja0117579 CCC: $22.00** 

***Table 1.*** Calculated Structures (Bond Distances/Å and Bond Angles/deg) and Energies (kcal/mol) for $Al^+(H_2O)$, $Al^+(H_2O)_4$, and $H_5O_2^+$ Clusters

| | VASP[a] | | | | |
|---|---|---|---|---|---|
| | set I | set II | Bauschlicher[b] | Iwata[c] | Schwarz[d] |
| $Al^+\cdots(H_2O)$ | | | | | |
| Al−O | 2.049 | 2.066 | 2.080 | 2.081 | 2.078 |
| O−H | 0.998 | 0.981 | | 0.981 | 0.972 |
| binding energy | 30.6 | 28.6 | 28.6 | 29.9 | 28.8 |
| $Al^+\cdots(H_2O)_4$ | | | | | |
| Al−O1 | 2.064 | 2.094 | | 2.186 | |
| Al−O2 | 2.098 | 2.129 | | 2.096 | |
| O···H | 1.775 | 1.808 | | 1.857 | |

$H_5O_2^+$ ($H_2O\cdots H^+\cdots OH_2$) $C_2$ Symmetry

| level of theory | basis set | $H^+\cdots O$ | O···O | H–O | O–$H^+$–O |
|---|---|---|---|---|---|
| HF | 6-31G* | 1.191 | 2.380 | 0.957 | 174.9 |
| | 6-31G** | 1.181 | 2.362 | 0.950 | 176.8 |
| | 6-311G** | 1.180 | 2.359 | 0.949 | 176.6 |
| MP2 | 6-31G* | 1.210 | 2.415 | 0.979 | 173.0 |
| | 6-31G** | 1.194 | 2.384 | 0.969 | 174.2 |
| | 6-311G** | 1.191 | 2.378 | 0.966 | 174.0 |
| BPW91 | 6-31G* | 1.219 | 2.433 | 0.983 | 172.8 |
| | 6-31G** | 1.209 | 2.414 | 0.978 | 173.7 |
| | 6-311G** | 1.206 | 2.409 | 0.975 | 173.9 |
| BLYP | 6-31G* | 1.225 | 2.444 | 0.987 | 172.6 |
| | 6-31G** | 1.215 | 2.426 | 0.981 | 173.4 |
| | 6-311G** | 1.211 | 2.418 | 0.978 | 174.0 |
| B3LYP | 6-31G* | 1.209 | 2.413 | 0.977 | 173.1 |
| | 6-31G** | 1.200 | 2.397 | 0.971 | 174.3 |
| | 6-311G** | 1.197 | 2.391 | 0.968 | 174.8 |
| VASP/PW91 | Set I | 1.198 | 2.393 | 0.992 | 175.2 |
| | Set II | 1.205 | 2.407 | 0.978 | 174.2 |

Proton-Transfer Barrier at O···O Distance of 2.74 Å (Gaussian Result $H_5O_2^+$ Fixed at $C_s$ Symmetry[e])

| | Gaussian[e] | | | | | VASP[a] | |
|---|---|---|---|---|---|---|---|
| level of theory | HF | MP2 | BP86 | BLYP | B3LYP | set I | set II |
| barrier | 9.64 | 4.56 | 1.41 | 1.49 | 2.97 | 2.60 | 2.63 |

[a] Set I: planewave cutoff energy 270 eV. Set II: planewave cutoff energy 396 eV. [b] Reference 36. [c] Reference 30. [d] Reference 32. [e] Reference 66.

theory,[30−41] and a partial list of the central ions includes the metals of main group I,[9−13,39−41] II,[14−22,35−38] and III,[23−27,30−34] as well as transition metals.[28,29]


(21) Woodward, C. A.; Dobson, M. P.; Stace, A. J. *J. Phys. Chem. A* **1997**, *101*, 2279.
(22) Beyer, M.; Williams, E. R.; Bondybey, V. E. *J. Am. Chem. Soc.* **1999**, *121*, 1565.
(23) Beyer, M.; Berg, C.; Gorlitzer, H. W.; Schindler, T.; Achatz, U.; Albert, G.; Niedner-Schatteburg, G.; Bondybey, V. E. *J. Am. Chem. Soc.* **1996**, *118*, 7386.
(24) Beyer, M.; Achatz, U.; Berg, C.; Joos, S.; Niedner-Schatteburg, G.; Bondybey, V. E. *J. Phys. Chem. A* **1999**, *103*, 671.
(25) Fuke, K.; Misaizu, F.; Sanekata, M.; Tsukamoto, K. Iwata, S. *Z. Phys. D: At., Mol. Clusters* **1993**, *26*, 180.
(26) Misaizu, F.; Tsukamoto, K.; Sanekata, M.; Fuke, K.; Iwata, S. *Z. Phys. D: At., Mol. Clusters* **1993**, *26*, 177.
(27) Misaizu, F.; Tsukamoto, K.; Sanekata, M.; Fuke, K. *Chem. Phys. Lett.* **1992**, *188*, 241.
(28) Misaizu, F.; Tsukamato, K.; Sanekata, M.; Fuke, F. *Laser Chem.* **1995**, *15*, 195.
(29) Thompson, C. J.; Husband, J.; Aguirre, F.; Metz, R. B. *J. Phys. Chem. A* **2000**, *104*, 8155.
(30) Watanabe, H.; Iwata, S. *J. Phys. Chem.* **1996**, *100*, 3377.
(31) Watanabe, H.; Aoki, M.; Iwata, S. *Bull. Chem. Soc. Jpn.* **1993**, *66*, 3245.
(32) Hrušák, J.; Stöckigt, D.; Schwarz, H. *Chem. Phys. Lett.* **1994**, *221*, 518.
(33) Sodupe, M.; Bauschlicher, C. W., Jr. *Chem. Phys. Lett.* **1991**, *181*, 321.
(34) Bauschlicher, C. W., Jr.; Partridge, H. *J. Phys. Chem.* **1991**, *95*, 9694.
(35) Bauschlicher, C. W., Jr.; Partridge, H. *J. Phys. Chem.* **1991**, *95*, 3946.
(36) Sodupe, M.; Bauschlicher, C. W., Jr. *Chem. Phys. Lett.* **1991**, *181*, 494.
(37) Bauschlicher, C. W., Jr.; Sodupe, M.; Partridge, H. *J. Chem. Phys.* **1992**, *96*, 4453.
(38) Watanabe, H.; Iwata, S.; Hashimoto, K.; Misaizu, F.; Fuke, K. *J. Am. Chem. Soc.* **1995**, *117*, 755.
(39) Bauschlicher, C. W., Jr.; Langoff, S. R.; Partridge, H.; Rice, J. E.; Komornicki, A. *J. Chem. Phys.* **1991**, *95*, 5142.
(40) Cabarcos, O. M.; Weinheimer, C. J.; Lisy, J. M. *J. Phys. Chem. A* **1999**, *103*, 8777.
(41) Cabarcos, O. M.; Lisy, J. M. *Chem. Phys. Lett.* **1996**, *257*, 265.


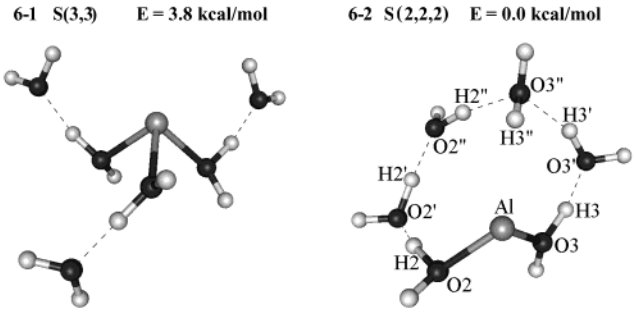


***Figure 1.*** Structures of $Al^+(H_2O)_6$ obtained by energy minimization using the VASP program. A certain shell structure is labeled by S(*l*, *n*, *m*, ...), with *l*, *n*, *m*, ... indicating the number of $H_2O$ molecules in the first, second, third, ... solvation shell. The initial geometry is generated by filling each solvation shell accordingly. An equilibration AIMD run is then performed for 2000 time steps (0.8 ps), and several configurations in this trajectory are randomly picked as the starting geometry for energy minimization. The structures shown in the figure are the ones with the lowest energies, the values of which are relative to the most stable structure. For structure parameters, please refer to Tables 2−4.

The subject of the present study, the ionic $Al^+(H_2O)_n$ cluster, is a typical example of such systems, in terms of the size-dependence effects. The stability of $Al^+(H_2O)_n$ varies with the cluster size as determined by two processes. The first is the evaporation of the solvent water molecules.[24] This is a cooling process because the clusters are produced by the collision of the metal ion plasma, often generated by laser vaporization, with water vapor, and thus there is a considerable amount of internal

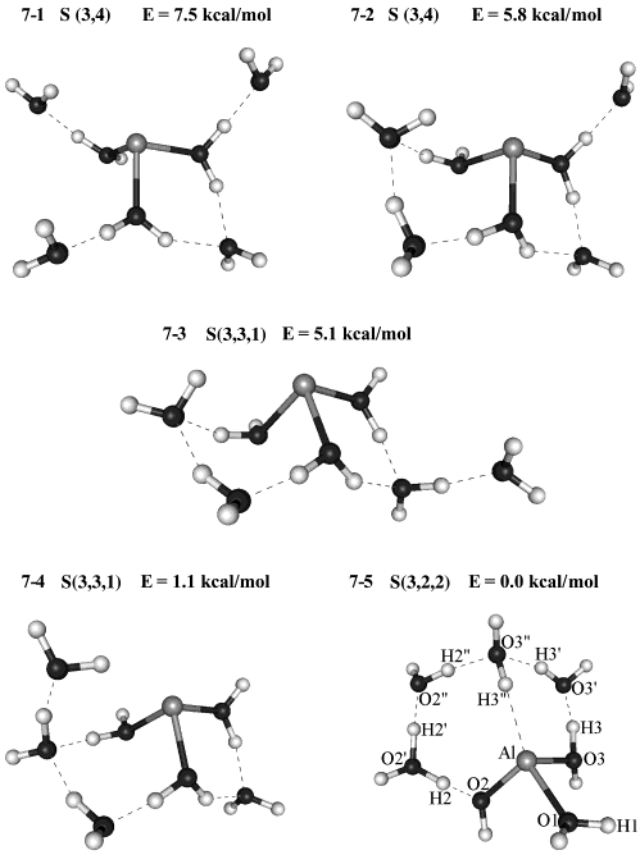


***Figure 2.*** Structures of $Al^+(H_2O)_7$ obtained by energy minimization using the VASP program. For the notations and the optimization method, please refer to the caption for Figure 1.

energy that could be dissipated by evaporation. In terms of chemistry, the second process is more interesting[23,24]

$$Al^+(H_2O)_n \rightarrow Al(OH)^+{}_2(H_2O)_{n-2} + H_2 \qquad (1)$$

in which a hydrogen molecule $H_2$ is eliminated by an intracluster reaction. The occurrence of reaction 1 is in the size region of $n = 11-24$. In other words, the reaction is not observed for the small clusters with $n < 11$ and for the large clusters with $n > 24$. Such phenomena of an intracluster reaction switched on and then off as the cluster size grows have been found before for other solvated metal ion clusters. For example, an intracluster reaction with the elimination of a hydrogen atom was observed for $Mg^+(H_2O)_n$[14,15] and $Mg^+(CH_3OH)_n$ clusters,[18] which was switched on around $n = 6$ and off around $n = 14$. Similar reactions and size-dependence effects have also been found for other alkaline earth metal ions.[15,18] The methanol clusters of sodium or cesium ions, $M^+(CH_3OH)_n$, showed another distinct type of size-dependent reaction, in which a dimethyl ether was formed and then eliminated.[9,10,13]

In the case of $Mg^+$ clusters, the size-dependence effects could be explained by thermodynamics. The hydration energy for the $(MgOH)^+$ ion core is higher than that for $Mg^+$, and as the number of solvent water increases to around $n = 6$, $(MgOH)^+(H_2O)_{n-1}$ becomes more stable than $Mg^+(H_2O)_n$.[14,18,38] When hydrogen is replaced by deuterium, the changes in the vibration frequencies would induce changes in zero-point energy and shift the switching size.[18,38] On the other hand, the understanding of the mechanism for these size-dependent reactions is very limited,

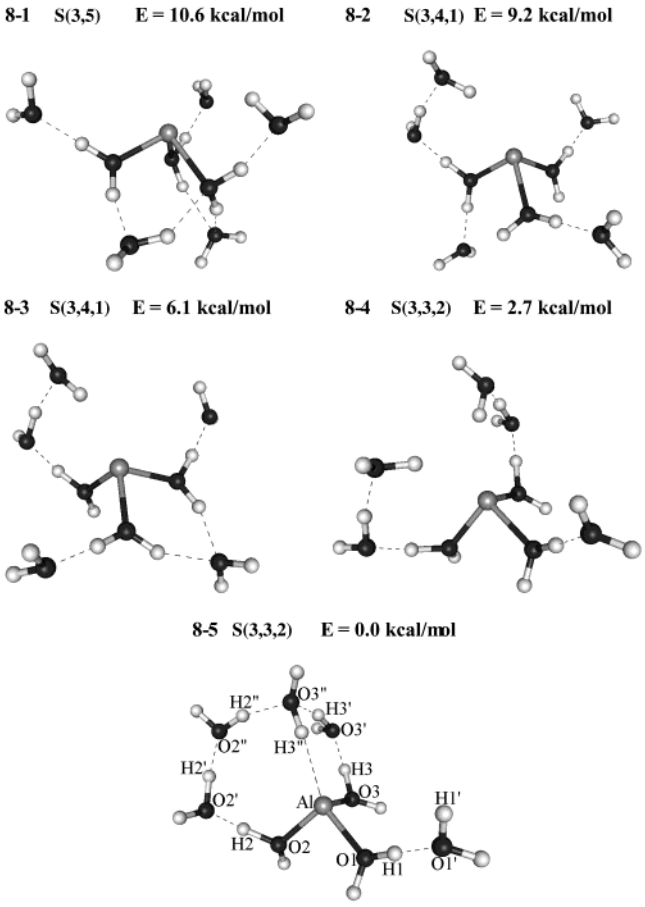


***Figure 3.*** Structures of $Al^+(H_2O)_8$ obtained by energy minimization using the VASP program. For the notations and the optimization method, please refer to the caption for Figure 1.

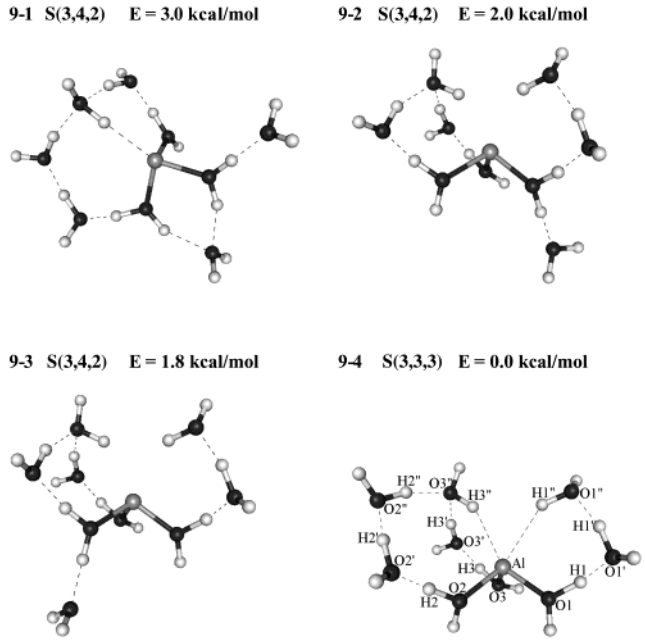


***Figure 4.*** Structures of $Al^+(H_2O)_9$ obtained by energy minimization using the VASP program. For the notations and the optimization method, please refer to the caption for Figure 1.

despite its obvious importance, because the calculation of the activation barrier for clusters of such sizes is quite a challenge. For example, it is known that there is an isomer to the $Al^+$-

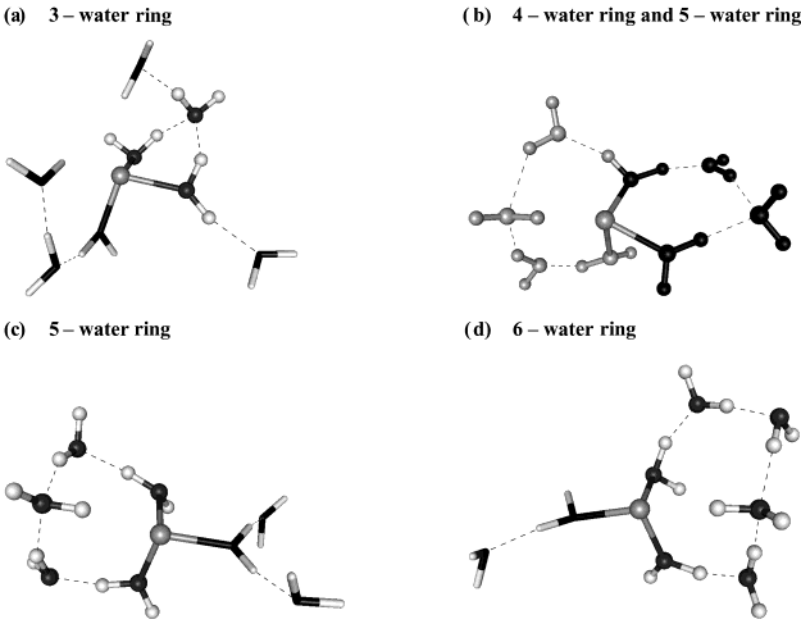


***Figure 5.*** Various ring structures observed for $Al^+(H_2O)_8$ in VASP optimized geometries and during AIMD simulations. These rings always involve the $Al^+$, together with a number of $H_2O$ molecules ($n = 3-6$), connected by hydrogen bonds.

$(H_2O)_n$ cluster in the form of $HAlOH^+(H_2O)_{n-1}$. For $n = 2$, the $HAlOH^+(H_2O)$ cluster is 19.82 kcal/mol (82.93 kJ/mol) more stable than its $Al^+(H_2O)_2$ isomer, and the energy difference favors $HAlOH^+(H_2O)_{n-1}$ further with increasing $n$.[30] However, there is considerable uncertainty about the role of $HAlOH^+(H_2O)_{n-1}$ clusters[24] in the intracluster reaction because there is an energy barrier to the insertion of $Al^+$ into the H−O bond in a $H_2O$ molecule. For $Al^+(H_2O)$, the barrier is at a hefty value of 63.8 kcal/mol,[32] and how the barrier changes with increasing cluster size has not been studied, to the best of our knowledge. The size-dependent $H_2$ elimination reaction in the $Al^+(H_2O)_n$ cluster cannot be fully understood on the basis of energy difference alone, without the knowledge of the transformation barriers between $Al^+(H_2O)_n$ and $HAlOH^+(H_2O)_{n-1}$.

Computational studies on small ionic clusters ($n < 6$) by ab initio methods have been widely reported in the literature,[30−39] and, in the case of $Al^+(H_2O)_n$, a great deal has been learned about the bonding interactions and cluster structures.[30−34] Similar to the $Mg^+(H_2O)_n$ clusters,[34−38] the interaction between $Al^+$ and $H_2O$ is electrostatic in nature with a slightly larger ligand to metal charge donation for Al than for Mg.[33] The $3s^2$ electrons are polarized away from the water ligands and act like a lone pair, resulting in repulsion among the lone pair and the ligands.[34] The maximum number of $H_2O$ molecules directly bonded to $Al^+$ is 3. For $Al^+(H_2O)_n$ with $n = 3$ and 4, the energy gain for the formation of a hydrogen bond connected ring could be larger than that of the $Al^+-H_2O$ bond, and there exists a stable dimer core structure with two $H_2O$ molecules in the first shell.[30]

In contrast, there is a large gap in our knowledge about the metal ion solvent clusters with sizes larger than 6. This is especially unfortunate for the $Al^+(H_2O)_n$ clusters as reaction 1 starts around $n = 11$.[23,24] Ab initio studies on these clusters are difficult because the computational cost rises fast with the increasing cluster size. More importantly, these cluster ions are bonded by the relatively weak hydrogen bonds. As a result, there are many shallow local minima on a flat multidimensional potential surface. The understanding of these clusters depends more on their dynamic behaviors rather than on their stationary structures. Classical molecular dynamics (MD) simulation helps in this aspect, as shown by Lisy and co-workers,[40,41] giving dynamics information about the shell extent, the occupation number in each shell, and the fragmentation patterns upon collision. Yet such a method cannot satisfactorily deal with the size-dependent chemical reactions.

In this paper, we report a computational study on $Al^+(H_2O)_n$, with $n = 6-14$. We used for our study the density functional theory (DFT) based ab initio molecular dynamics method (AIMD) with a planewave basis set, pseudopotentials for core electrons, and direct minimization of the total energy over the planewave coefficients.[42−46] Because of its remarkable computational efficiency, this method has been widely used for the study of large sized systems and for the solvation dynamics in clusters and solutions.[46] The forces and potential energy needed for molecular dynamics integration are obtained directly from DFT calculation at each time step. For ion−solvent clusters such as $Al^+(H_2O)_n$, direct sampling of the phase space from first principles provides a powerful tool to locate the manifold of structures that lie closely to each other in energy, to understand their stability and the transformation among them, and, more importantly, to reveal intracluster reactions and to offer valuable leads to the location of reaction barriers. Examples of such studies have already been reported in the literature for $Al^{3+}(H_2O)_n$,[47] $Be^{2+}$ in aqueous solution,[48] and the aqueous proton cluster $H^+(H_2O)_n$.[49−52]

(42) Car, R.; Parrinello, M. *Phys. Rev. Lett.* **1985**, *55*, 2471.
(43) Parrinello, M. *Solid State Commun.* **1997**, *102*, 107.
(44) Remler, D. K.; Madden, P. A. *Mol. Phys.* **1990**, *70*, 921.
(45) Payne, M. C.; Teter, M. P.; Allan, D. C.; Arias, T. A.; Joannopoulos, J. D. *Rev. Mod. Phys.* **1992**, *64*, 1045.
(46) Tuckerman, M. E.; Ungar, P. J.; Vonrosenvinge, T.; Klein, M. L. *J. Phys. Chem.* **1996**, *100*, 12878.
(47) Lubin, M. I.; Bylaska, E. J.; Weare, J. H. *Chem. Phys. Lett.* **2000**, *322*, 447.
(48) Marx, D.; Sprik, M.; Parrinello, M. *Chem. Phys. Lett.* **1997**, *273*, 360.
(49) Cheng, H. P.; Krause, J. L. *J. Chem. Phys.* **1997**, *107*, 8461.
(50) Wei, D. Q.; Salahub, D. R. *J. Chem. Phys.* **1997**, *106*, 6086.
(51) Marx, D.; Tuckerman, M. E.; Hutter, J.; Parrinello, M. *Nature* **1999**, *397*, 601.

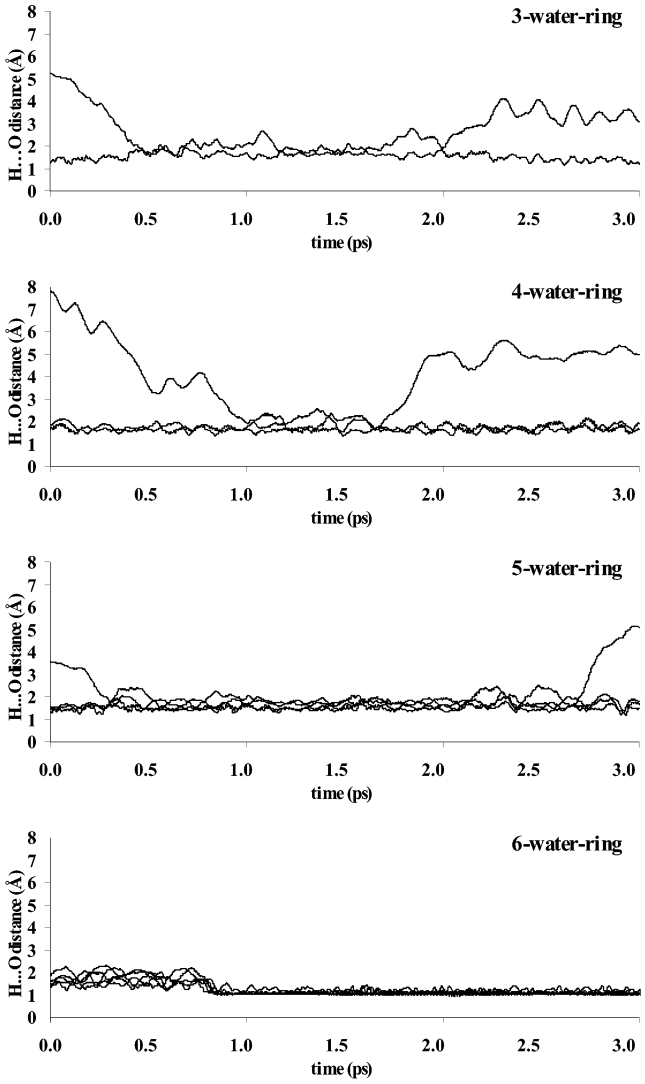


***Figure 6.*** The fluctuation in the distances of hydrogen bonds connecting the ring structures in Figure 5, during AIMD simulations on $Al^+(H_2O)_8$ isomers at 300 K. A hydrogen bond is broken when its distance value is significantly higher than 2 Å. Only the six-water-ring is stable during the entire duration of the 3 ps AIMD simulation.

## Computational Methods

The principles of AIMD method have been documented in the literature[42−46] and will not be reproduced here. We use the VASP (Vienna Ab Initio Simulation Package), developed at the Institut für Theoretische Physik of the Technische Universität Wien,[53−56] for our trajectory studies. An $Al^+(H_2O)_n$ cluster is put in a cubic box to imitate gas-phase conditions, and the lattice length is 14 Å for $n = 6-10$, and 16 Å for $n > 10$. A planewave basis set with a cutoff energy of 270 eV is used for the electron wave function, which is solved at each MD step by RMM-DIIS minimization of the total electronic energy. The Perdew−Wang[57] gradient correction (PW91) is added to the exchange-correlation functional.[58] For the core region, the optimized Vanderbilt ultrasoft pseudopotentials[59] supplied with the VASP package[60,61] are directly used. In the AIMD simulation, the time step used is 0.4 fs, and the temperature is controlled by a Nośe−Hoover thermostat.[62,63] Good energy conservation, including the kinetic and potential energy for both the cluster and the thermostat, is observed in all simulations.

***Table 2.*** Geometry Parameters (Bond Distances/Å and Bond Angles/deg) for VASP Optimized Structures Corresponding to **6-2**, **7-5**, **8-5**, and **9-4**

| | 6-2 | 7-5 | 8-5 | 9-4 |
|---|---|---|---|---|
| Al−O1 | | 2.029 | 1.952 | 1.852 |
| Al−O2 | 1.866 | 1.828 | 1.885 | 1.867 |
| Al−O3 | 1.902 | 1.946 | 1.955 | 1.942 |
| Al−H3″ | 2.460 | 2.128 | 2.190 | 2.303 |
| Al−H1″ | | | | 2.444 |
| O1−H1 | | 0.996 | 1.044 | 1.168 |
| O2−H2 | 1.204 | 1.292 | 1.155 | 1.141 |
| O3−H3 | 1.080 | 1.084 | 1.077 | 1.072 |
| O1′−H1 | | | 1.510 | 1.258 |
| O2′−H2 | 1.226 | 1.148 | 1.278 | 1.278 |
| O3′−H3 | 1.411 | 1.416 | 1.429 | 1.435 |
| O1′−H1′ | | | 0.991 | 1.058 |
| O2′−H2′ | 1.055 | 1.099 | 1.056 | 1.054 |
| O3′−H3′ | 1.014 | 1.023 | 1.024 | 1.023 |
| O1″−H1′ | | | | 1.478 |
| O2″−H2′ | 1.482 | 1.355 | 1.477 | 1.470 |
| O3″−H3′ | 1.761 | 1.698 | 1.684 | 1.683 |
| O3″−H2″ | 1.762 | 1.602 | 1.645 | 1.686 |
| O1″−H1″ | | | | 1.032 |
| O2″−H2″ | 1.012 | 1.032 | 1.023 | 1.018 |
| O3″−H3″ | 1.023 | 1.087 | 1.075 | 1.062 |
| O1−Al−O2 | | 93.8 | 94.6 | 100.6 |
| O2−Al−O3 | 92.4 | 102.7 | 95.8 | 92.7 |
| O3−Al−O1 | | 87.7 | 94.9 | 96.7 |
| Al−H3″−O3″ | 136.6 | 151.3 | 151.5 | 146.2 |

Table 1 shows the energies and structure parameters obtained by VASP calculations for $Al^+(H_2O)$, $Al^+(H_2O)_4$, and $H^+(H_2O)_2$, together with previous results reported in the literature. For $Al^+(H_2O)$, the binding energy is in good agreement with previously reported values,[30,32] as are most of the structural parameters for all three clusters. The largest deviation from Hartree−Fock based calculations is in the energy barrier for the proton transfer in $H^+(H_2O)_2$, which is well known for various types of DFT functionals.[64−66] We have thus performed additional calculations for a few selected $Al^+(H_2O)_n$ clusters, using the Gaussian 98 program,[67] at both the DFT/BPW91 and the Hartree−Fock/MP2 levels with basis sets of 6-31G* and 6-31G**. For these calculations, stable and transition structures are verified by obtaining the vibrational frequencies. On the other hand, the results from the present planewave method using PW91 are in very good agreement with those obtained by Gaussian based BPW91 and B3LYP calculations. Furthermore, we observe only minor differences between the results (geometry and energy) obtained from a planewave cutoff of 270 eV (set I) with those using a larger energy cutoff of 396 eV (set II).

(52) Tuckerman, M. E.; Marx, D.; Klein, M. L.; Parrinello, M. *Science* **1997**, *275*, 817.
(53) Kresse, G.; Furthmüller, J. *Phys. Rev. B* **1996**, *54*, 11169.
(54) Kresse, G.; Hafner, J. *Phys. Rev. B* **1993**, *47*, 558.
(55) Kresse, G.; Hafner, J. *Phys. Rev. B* **1991**, *49*, 14251.
(56) Kresse, G.; Furthmüller, J. *Comput. Mater. Sci.* **1996**, *6*, 15.
(57) Perdew, J. P. In *Electronic Structure of Solids '91*; Ziesche, P., Eschrig, H., Eds.; Academie Verlag: Berlin, 1991; p 11.
(58) Perdew, J. P.; Zunger, A. *Phys. Rev. B* **1981**, *23*, 5048.
(59) Vanderbilt, D. *Phys. Rev. B* **1990**, *41*, 7892.
(60) Kresse, G.; Hafner, J. *J. Phys.: Condens. Matter* **1994**, *6*, 8245.
(61) Kresse, G.; Hafner, J. *Phys. Rev. B* **1993**, *48*, 13115.
(62) Nosé, S. *J. Chem. Phys.* **1984**, *81*, 511.
(63) Hoover, W. G. *Phys. Rev. A* **1985**, *31*, 1695.
(64) Sadhukhan, S.; Muñoz, D.; Adamo, C.; Scuseria, G. E. *Chem. Phys. Lett.* **1999**, *306*, 83.
(65) Paves, M.; Chawla, S.; Lu, D.; Lobaugh, J.; Voth, G. A. *J. Chem. Phys.* **1997**, *107*, 7428.
(66) Barone, V.; Orlandini, L.; Adamo, C. *Chem. Phys. Lett.* **1994**, *231*, 295.
(67) Frisch, M. J.; Trucks, G. W.; Schlegel, H. B.; Scuseria, G. E.; Robb, M. A.; Cheeseman, J. R.; Zakrzewski, V. G.; Montgomery, J. A.; Stratmann, R. E.; Burant, J. C.; Dapprich, S.; Millam, J. M.; Daniels, A. D.; Kudin, K. N.; Strain, M. C.; Farkas, O.; Tomasi, J.; Barone, V.; Cossi, M.; Cammi, R.; Mennucci, B.; Pomelli, C.; Adamo, C.; Clifford, S.; Ochterski, J.; Petersson, G. A.; Ayala, P. Y.; Cui, Q.; Morokuma, K.; Malick, D. K.; Rabuck, A. D.; Raghavachari, K.; Foresman, J. B.; Cioslowski, J.; Ortiz, J. V.; Baboul, A. G.; Stefanov, B. B.; Liu, G.; Liashenko, A.; Piskorz, P.; Komaromi, I.; Gomperts, R.; Martin, R. L.; Fox, D. J.; Keith, T.; Al-Laham, M. A.; Peng, C. Y.; Nanayakkara, A.; Gonzalez, C.; Challacombe, M.; Gill, P. M. W.; Johnson, B.; Chen, W.; Wong, M. W.; Andres, J. L.; Gonzalez, C.; Head-Gordon, M.; Replogle, E. S.; Pople, J. A. *Gaussian 98*; Gaussian, Inc.: Pittsburgh, PA, 1998.

***Table 3.*** Geometry Parameters (Bond Distances/Å and Bond Angles/deg) for BPW91 Optimized Structures Corresponding to **6-2**, **7-5**, **8-5**, and **9-4**

| | **6-2** | | **7-5** | | **8-5** | | **9-4** | |
|---|---|---|---|---|---|---|---|---|
| | 6-31G* | 6-31G** | 6-31G* | 6-31G** | 6-31G* | 6-31G** | 6-31G* | 6-31G** |
| Al−O1 | | | 2.111 | 2.110 | 2.011 | 2.005 | 1.952 | 1.942 |
| Al−O2 | 2.037 | 2.030 | 1.947 | 1.930 | 1.964 | 1.952 | 1.941 | 1.928 |
| Al−O3 | 1.957 | 1.953 | 2.018 | 2.014 | 2.021 | 2.014 | 1.993 | 1.984 |
| Al−H3″ | 3.787 | 3.773 | 2.444 | 2.444 | 2.376 | 2.371 | 2.418 | 2.411 |
| Al−H1″ | | | | | | | 2.590 | 2.565 |
| O1−H1 | | | 0.984 | 0.979 | 1.027 | 1.026 | 1.092 | 1.102 |
| O2−H2 | 1.018 | 1.016 | 1.106 | 1.121 | 1.090 | 1.102 | 1.097 | 1.109 |
| O3−H3 | 1.032 | 1.032 | 1.053 | 1.055 | 1.050 | 1.050 | 1.054 | 1.055 |
| O1′−H1 | | | | | 1.592 | 1.560 | 1.405 | 1.365 |
| O2′−H2 | 1.652 | 1.623 | 1.375 | 1.327 | 1.408 | 1.363 | 1.390 | 1.347 |
| O3′−H3 | 1.571 | 1.539 | 1.517 | 1.482 | 1.527 | 1.496 | 1.506 | 1.474 |
| O1′−H1′ | | | | | 0.978 | 0.974 | 1.021 | 1.022 |
| O2′−H2′ | 1.027 | 1.027 | 1.025 | 1.027 | 1.023 | 1.024 | 1.024 | 1.026 |
| O3′−H3′ | 0.988 | 0.984 | 1.000 | 0.997 | 1.002 | 0.999 | 1.003 | 0.999 |
| O1″−H1′ | | | | | | | 1.638 | 1.606 |
| O2″−H2′ | 1.597 | 1.567 | 1.605 | 1.563 | 1.617 | 1.579 | 1.611 | 1.571 |
| O3″−H3′ | 1.930 | 1.946 | 1.797 | 1.788 | 1.789 | 1.786 | 1.778 | 1.772 |
| O3″−H2″ | 1.884 | 1.885 | 1.830 | 1.831 | 1.825 | 1.819 | 1.825 | 1.817 |
| O1″−H1″ | | | | | | | 0.999 | 0.998 |
| O2″−H2″ | 0.992 | 0.988 | 0.995 | 0.991 | 0.996 | 0.992 | 0.995 | 0.992 |
| O3″−H3″ | 0.979 | 0.975 | 1.011 | 1.008 | 1.021 | 1.018 | 1.020 | 1.018 |
| O1−Al−O2 | | | 88.8 | 89.7 | 88.7 | 89.4 | 93.4 | 94.5 |
| O2−Al−O3 | 83.3 | 83.3 | 89.2 | 90.8 | 88.0 | 89.0 | 90.7 | 91.9 |
| O3−Al−O1 | | | 83.5 | 83.5 | 88.8 | 89.4 | 90.1 | 90.9 |
| Al−H3″−O3″ | 129.1 | 129.0 | 144.5 | 143.9 | 148.9 | 148.6 | 148.5 | 148.4 |

***Table 4.*** Geometry Parameters (Bond Distances/Å and Bond Angles/deg) for MP2 Optimized Structures Corresponding to **8-5** and **9-4**

| | **8-5** | | **9-4** | |
|---|---|---|---|---|
| | 6-31G* | 6-31G** | 6-31G* | 6-31G** |
| Al−O1 | 2.015 | 2.014 | 1.980 | 1.975 |
| Al−O2 | 1.989 | 1.982 | 1.974 | 1.966 |
| Al−O3 | 2.039 | 2.038 | 2.019 | 2.016 |
| Al−H3″ | 2.651 | 2.633 | 2.676 | 2.656 |
| Al−H1″ | | | 3.001 | 2.946 |
| O1−H1 | 1.005 | 0.999 | 1.034 | 1.034 |
| O2−H2 | 1.035 | 1.035 | 1.036 | 1.037 |
| O3−H3 | 1.016 | 1.010 | 1.017 | 1.012 |
| O1′−H1 | 1.654 | 1.616 | 1.526 | 1.476 |
| O2′−H2 | 1.527 | 1.472 | 1.520 | 1.464 |
| O3′−H3 | 1.612 | 1.575 | 1.601 | 1.562 |
| O1′−H1′ | 0.972 | 0.964 | 0.992 | 0.986 |
| O2′−H2′ | 0.994 | 0.989 | 0.995 | 0.989 |
| O3′−H3′ | 0.985 | 0.977 | 0.985 | 0.977 |
| O1″−H1′ | | | 1.746 | 1.718 |
| O2″−H2′ | 1.723 | 1.689 | 1.721 | 1.686 |
| O3″−H3′ | 1.875 | 1.869 | 1.871 | 1.863 |
| O3″−H2″ | 1.915 | 1.910 | 1.917 | 1.911 |
| O1″−H1″ | | | 0.975 | 0.969 |
| O2″−H2″ | 0.980 | 0.972 | 0.980 | 0.972 |
| O3″−H3″ | 0.987 | 0.980 | 0.957 | 0.980 |
| O1−Al−O2 | 84.9 | 85.5 | 87.4 | 88.3 |
| O2−Al−O3 | 84.0 | 84.4 | 85.5 | 86.3 |
| O3−Al−O1 | 85.0 | 85.3 | 85.5 | 86.0 |
| Al−H3″−O3″ | 142.9 | 142.6 | 143.8 | 143.6 |

## Results and Discussion

**$Al^+(H_2O)_n$ Shell Structures for $n = 6-9$.** The structures of $Al^+(H_2O)_n$ for $n = 6-9$ are illustrated in Figures 1−4. In searching for these structures, several possible initial geometries are first generated. According to a previous study on $Al^+(H_2O)_n$, $n = 2-5$, the $Al^+$ could be directly bonded to only two or three water molecules in the first solvation shell,[30] and, because of the presence of the polarized lone electron pair on $Al^+$, the maximum coordination number is 3.[34] Each $H_2O$ molecule in the first shell could then take a maximum number of two more $H_2O$ molecules with hydrogen bonds. Our initial choices of $Al^+(H_2O)_n$ ($n = 6-9$) structures are obtained by varying the number of $H_2O$ molecules in the first, second, and third shells. Each structure is first equilibrated in an AIMD simulation for 2000 time steps at 100 K. Several configurations are then randomly picked from this AIMD run as the initial geometries for energy minimization, which includes a short thermal annealing of 500 time steps starting from 100 K, and then followed by quasi-Newton optimization. The structures with the lowest energies are shown in Figures 1−4. Each one of these structures is further subjected to an AIMD simulation of 3 ps (7500 time steps) at 300 K to test its stability. The evaporation of $H_2O$ molecules is only observed for **9-1**.

The dimer core structure, with two $H_2O$ molecules in the first shell, was found in a previous study to be the most stable isomer for $Al^+(H_2O)_n$, $n = 3$ and 4, while for $n = 5$, the trimer core structure was the most stable.[30] This trend continues for larger $n$, with the only exception for $n = 6$ (Figure 1), for which a dimer core structure **6-2**, connected by a 12-member ring with six $H_2O$ molecules and the $Al^+$, is the most stable. When four $H_2O$ molecules are put in the first shell, the structure is unstable and transforms itself into a trimer core structure during the short AIMD equilibration run at 100 K.

For the second solvation shell, the number of $H_2O$ molecules varies from 2 to 5 in the initial geometry chosen in our calculation. Generally, an occupation number larger than 3 is not energetically favorable, as in the examples of **7-1**, **8-1**, **8-2**, and **8-3**, due to two reasons. First, with an occupation number of 3 in an incomplete second shell, each first shell $H_2O$ is hydrogen bonded to one second shell $H_2O$, and exceeding that number may result in repulsion among second shell $H_2O$ molecules. More importantly, $H_2O$ molecules in the third shell

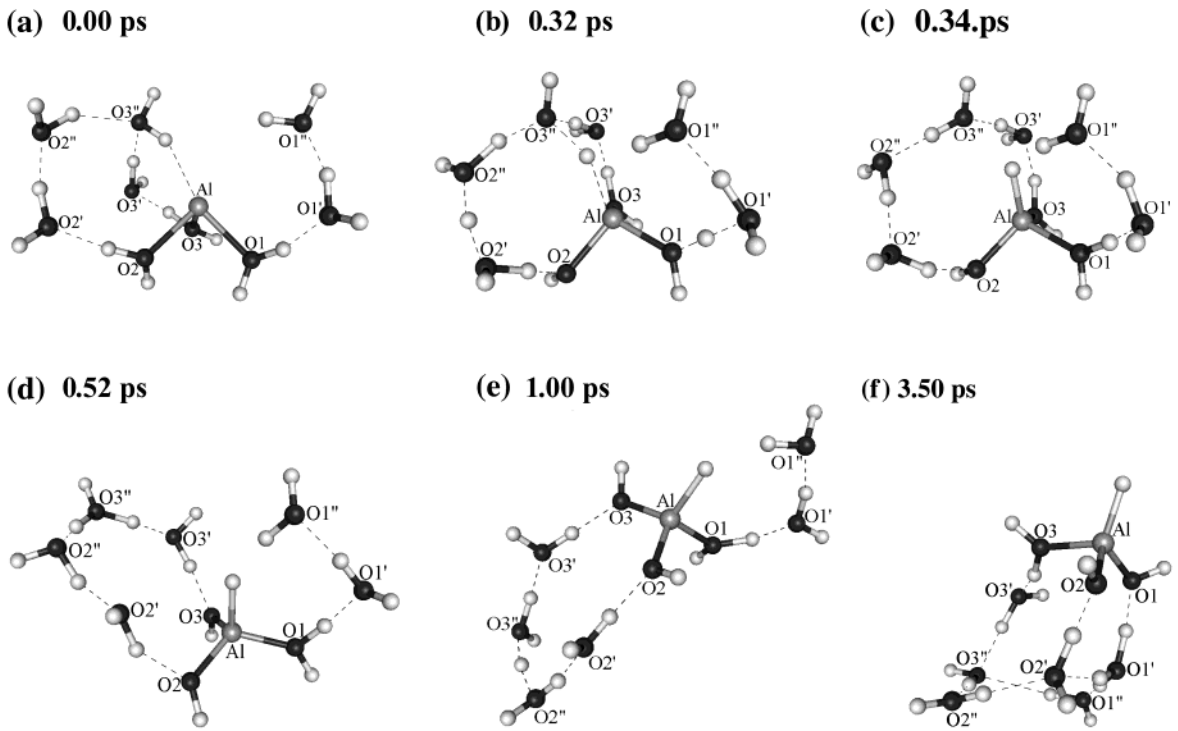


***Figure 7.*** Snapshots of an AIMD simulation on $Al^+(H_2O)_9$ (**9-4**) at 300 K. The isomerization reaction 2 starts around 0.32 ps and is complete by 0.52 ps.

Ⓦ A video in mpg format is available.

could form ring structures, connected by hydrogen bonds, with molecules in the first and second shells, and such rings could have a large stabilizing effect.

**$H_2O$ Ring Structures.** A three-water-ring, with six atomic members including $Al^+$, as shown in Figure 5a, was first suggested and studied by Watanabe and Iwata.[30] We observed other types of ring structures, formed spontaneously during the AIMD simulation at 300 K, with the number of $H_2O$ varying from 3 to 6, as shown in Figure 5 for $Al^+(H_2O)_8$. For three- and four-water-rings, only the first and second shell $H_2O$ molecules are involved, while the five- and six-water-rings involve $H_2O$ molecules in the first three shells.

Among these ring structures, the most remarkable is the six-water-ring (Figure 5d). For the optimized structures shown in Figures 1−4, the structure with the lowest energy for each $n$ always contains a six-water-ring in it. For $n = 6$ (**6-2**), it takes the form of a dimer core and is more stable than the trimer core **6-1**, indicating that the formation of such a ring is energetically more favorable than the formation of the third $Al^+-H_2O$ bond. Going from **7-5** to **8-5** and then to **9-4**, the six-water-ring remains intact, while the extra $H_2O$ molecules form a tail of the $H_2O$ chain.

Nonetheless, energy differences among isomers of the same size $n$ are on the order of only a few kcal/mol and do not tell us a lot about their solvation dynamics and stability, for which we have to rely on AIMD simulations. As shown in Figure 6 for $Al^+(H_2O)_8$, the fluctuation of the hydrogen bond distances during AIMD simulations at 300 K provides a good indication of the stability of various ring structures. The typical length of a hydrogen bond is below 2 Å, and a significant increase beyond that value indicates a breakdown of the ring structure. Both the three- and the four-water-rings are quite unstable. The five-water-ring is formed during the simulation and is stable for most part of the simulation, but breaks down near the end. In contrast, only the six-water-ring is stable for the entire 3 ps duration of the simulation. Similar patterns are observed for $n = 7$ and 9, with the only exception of $n = 6$ (**6-2**), for which the six-water-ring breaks down.

The structure parameters for **6-2**, **7-5**, **8-5**, and **9-4**, all containing a six-water ring, are listed in Table 2, as obtained by VASP calculation. The most notable feature is the fairly short O···H distance around 1.3−1.4 Å for the hydrogen bonds between the first and second shell $H_2O$ (the O2′−H2 and O3′−H3 distances), as compared to a more typical value of around 1.7−1.9 Å reported for the small $Al^+(H_2O)_n$ clusters ($n$ = 1−6).[30] The shortened distance is close to the previously reported average value in DFT based ab initio MD simulations for $H^+(H_2O)_n$[49,50] and indicates a strong acidic dissociation effect.

It is well known that DFT calculations often underestimate hydrogen bond distances and energy barriers for proton transfer through hydrogen bonded water clusters.[64−66] In our AIMD simulation, further approximation is introduced by the use of pseudopotentials. To verify the six-water-ring structure, further calculations were performed using the Gaussian based DFT method with BPW91 functional and the Hartree−Fock/MP2 method with 6-31G* and 6-31G** basis sets.

With BPW91/6-31G* (Table 3), all of the six-water-ring structures (**6-2**, **7-5**, **8-5**, and **9-4**) have been located and proved to be energy minima by frequency calculations. The difference in geometry parameters, as compared to the VASP results listed in Table 2, is small. Using $Al^+(H_2O)_9$ as an example, we found that the O2′−H2 distance increases from the VASP value of 1.28 Å to the BPW91/6-31G** value of 1.35 Å, while the O3′−H3 distance increases from 1.44 to 1.47 Å. In the MP2/6-31G** results (Table 4), the corresponding distances increase further

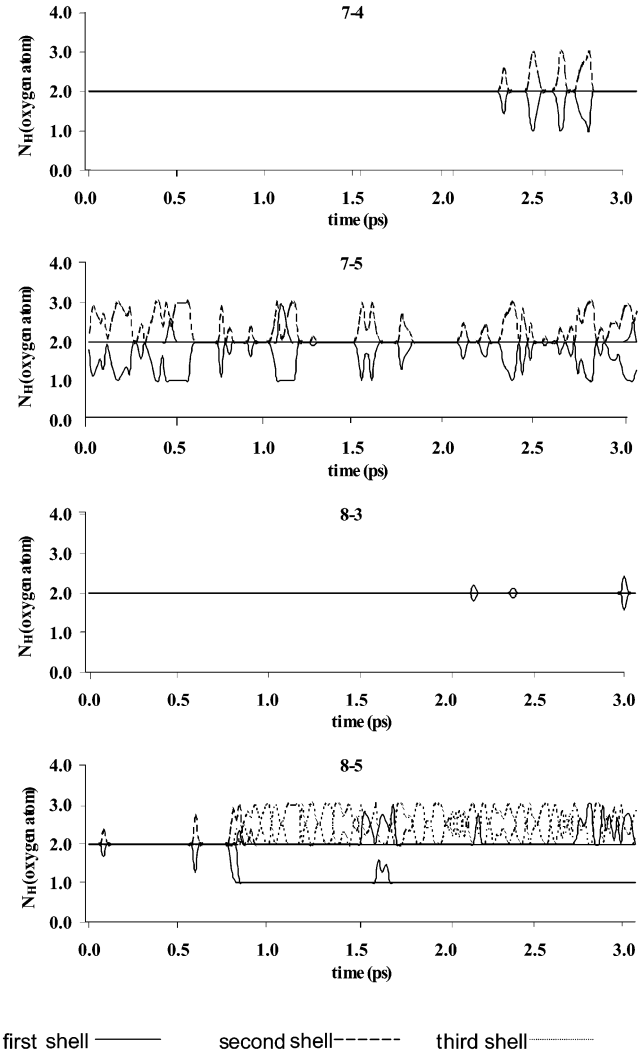


***Figure 8.*** Change in the coordination number of hydrogen atoms around an O atom as a function of time, during AIMD simulations on structures **7-4**, **7-5**, **8-3**, and **8-5**. When acidic dissociation occurs, the number decreases to 1. When a $H_2O$ molecule accepts a proton to become a hydronium ion, the number increases to 3. The fluctuation observed in the hydrogen coordination numbers is thus a good indication of the extent of acidic dissociation and proton transfer.

to 1.46 and 1.56 Å, respectively, which are still lower than the typical hydrogen bond distance. It indicates that although the VASP and DFT/BPW91 methods may overestimate the strength of hydrogen bonds, the interaction in the six-water-ring is stronger than average even in the MP2 results. However, our MP2 calculations only found stable six-water-ring structures for $n = 8$ and 9, not for $n = 6$ and 7. In our AIMD simulation, the six-water-ring in **6-2** also broke down at 300 K. It seems to indicate that **6-2** and **7-5** are not as stable as **8-5** and **9-4**. The latter two contain in their structures an extra chain of $H_2O$ molecules, which may be needed to stabilize the six-water-ring.

**Intracluster Insertion Reaction.** The most interesting feature of the six-water-ring is its role as a precursor to an intracluster reaction observed during the AIMD simulations at 300 K:

$$Al^+(H_2O)_n \rightarrow HAlOH^+(H_2O)_{n-1} \qquad (2)$$

The reaction mechanism is schematically shown in Figure 7 for $Al^+(H_2O)_9$. Within the six-water-ring, the water labeled by O3″ is in a unique position, as it forms two hydrogen bonds through O3″ only. All of the other $H_2O$ molecules contribute the O atom and one H atom to hydrogen bonds. One of the hydrogen atoms covalently bonded to O3″ is directly pointed at $Al^+$, with an Al−H distance of 2.7 Å at the MP2/6-31G** level. During the simulation at 300 K, this hydrogen atom is released as a proton to $Al^+$, due to acidic dissociation. It captures the electron lone pair on $Al^+$ and forms an Al−H hydride bond. In compensation, O3″ receives a proton from a neighboring $H_2O$ molecule. The reaction is similar to that for the monomer-core $B^+H_2O(H_2O)_{n-1}$ clusters, which is a barrierless process that requires three or more $H_2O$ molecules.[30] Among the structures shown in Figures 1−4, reaction 2 is only observed for clusters of a size $n \geq 8$ that contain a six-water-ring structure (**8-5** and **9-4**).

As discussed above, the short O···H distance in the six-water-ring indicates the presence of acidic dissociation. This process is crucial for the insertion reaction 2, and its extent can be seen from the change in the number of H atoms around O atoms. In Figure 8, the coordination number as a function of time is plotted for simulations starting with structures **7-4**, **7-5**, **8-3**, and **8-5**, respectively. The contrast between the clusters with a six-water-ring (**7-5**, **8-5**) and those without (**7-4**, **8-3**) is striking. For the former, there are extensive fluctuations in the H coordination numbers due to the acidic dissociation and the transfer of protons through the hydrogen bonded ring, while for the latter, the coordination numbers are almost constant, with only very short-lived fluctuations. The difference between **7-5** and **8-5** is that in the simulation for **8-5** the insertion reaction 2 takes place just below 1 ps, and, after the formation of $HAlOH^+(H_2O)_7$, the acidic dissociation is even more prominent.

With the insertion reaction revealed by AIMD simulation, transition structures for $n = 8$ and 9 (Figure 9 and Table 5) are also successfully located, by both the BPW91 and the MP2 methods. As shown in Table 6, the energy barriers obtained by the BPW91 method are around 7−8 kcal/mol lower than the barriers obtained by the MP2 method. This discrepancy is probably because of the fact that the intracluster reaction is associated with the acidic dissociation and the proton transfer around the six-water-ring, and DFT is known to underestimate the barrier for proton transfer.[64] Our best estimate of the reaction barriers are the MP2/6-31G** values with zero-point corrections included, at 7.1 kcal/mol for $n = 8$ and 10.0 kcal/mol for $n = 9$ (Table 6), much lower than the barrier of 63.8 kcal/mol for the formation of $HAlOH^+$ from $Al^+(H_2O)$.[32] A search for a similar transition structure for $n = 6$ and 7, using the BPW91/6-31G* method, was not successful. This is, however, in agreement with the AIMD simulation in which no $HAlOH^+(H_2O)_{n-1}$ formation is observed for **6-2** and **7-5**.

There are several interesting conclusions that we can draw from the results on $Al^+(H_2O)_n$, $n = 6-9$. First, the buildup of the shell structure around $Al^+$ is a complicated process. It is energetically preferable to leave the second solvation shell incomplete to reduce the repulsion among $H_2O$ molecules. Furthermore, $H_2O$ molecules may fill the third shell first so that ring structures connected by hydrogen bonds could be formed. Second, a size-dependent insertion reaction is switched on at $n = 8$ with $Al^+(H_2O)_n$ isomerizing into $HAlOH^+(H_2O)_{n-1}$ (reaction 2). Thermodynamically, $HAlOH^+(H_2O)_{n-1}$ is around

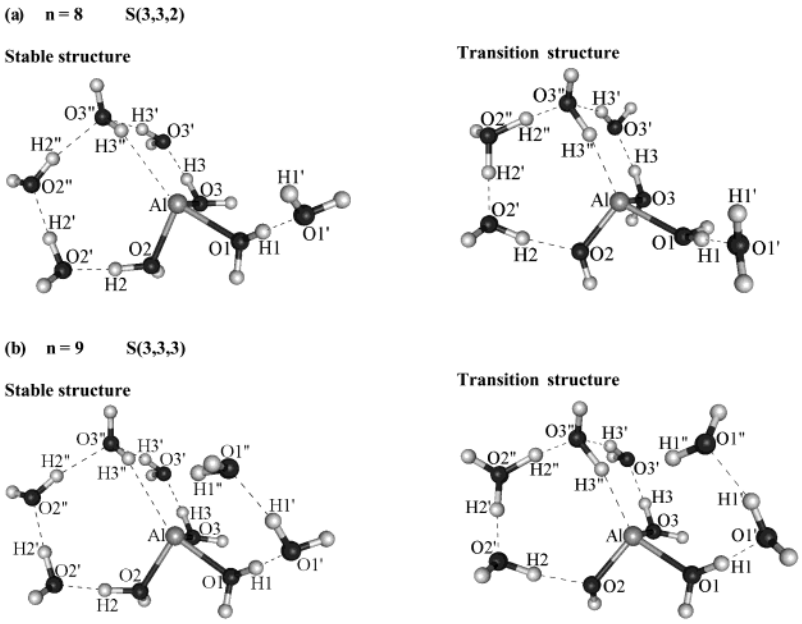


***Figure 9.*** The stable and transition structures for reaction 2, optimized at the MP2/6-31G** level, for $Al^+(H_2O)_n$, $n = 8$ and 9. Geometry parameters are listed in Table 5.

***Table 5.*** Geometry Parameters (Bond Distances/Å and Bond Angles/deg) of the Transition Structures for the Insertion Reaction, $n = 8$ and 9

| | 8-5 | | | | 9-4 | | | |
|---|---|---|---|---|---|---|---|---|
| | BPW91 | | MP2 | | BPW91 | | MP2 | |
| | 6-31G* | 6-31G** | 6-31G* | 6-31G** | 6-31G* | 6-31G** | 6-31G* | 6-31G** |
| Al−O1 | 1.992 | 1.983 | 1.989 | 1.985 | 1.935 | 1.920 | 1.960 | 1.950 |
| Al−O2 | 1.811 | 1.812 | 1.786 | 1.784 | 1.822 | 1.829 | 1.790 | 1.791 |
| Al−O3 | 2.009 | 1.993 | 2.037 | 2.030 | 1.947 | 1.928 | 1.989 | 1.981 |
| Al−H3″ | 2.006 | 1.977 | 2.095 | 2.053 | 1.964 | 1.939 | 2.095 | 2.047 |
| Al−H1″ | | | | | 2.607 | 2.594 | 2.825 | 2.811 |
| O1−H1 | 1.025 | 1.025 | 1.003 | 0.997 | 1.091 | 1.105 | 1.032 | 1.031 |
| O2−H2 | 1.516 | 1.484 | 1.686 | 1.653 | 1.468 | 1.403 | 1.679 | 1.638 |
| O3−H3 | 1.054 | 1.060 | 1.010 | 1.004 | 1.072 | 1.090 | 1.010 | 1.006 |
| O1′−H1 | 1.597 | 1.561 | 1.661 | 1.620 | 1.406 | 1.358 | 1.539 | 1.483 |
| O2′−H2 | 1.049 | 1.050 | 1.002 | 0.996 | 1.468 | 1.403 | 1.003 | 0.998 |
| O3′−H3 | 1.517 | 1.471 | 1.656 | 1.616 | 1.457 | 1.394 | 1.647 | 1.599 |
| O1′−H1′ | 0.977 | 0.973 | 0.971 | 0.963 | 1.020 | 1.021 | 0.992 | 0.985 |
| O2′−H2′ | 1.272 | 1.262 | 1.493 | 1.454 | 1.220 | 1.179 | 1.491 | 1.440 |
| O3′−H3′ | 1.006 | 1.005 | 0.980 | 0.972 | 1.014 | 1.019 | 0.980 | 0.973 |
| O1″−H1′ | | | | | 1.639 | 1.604 | 1.757 | 1.730 |
| O2″−H2′ | 1.177 | 1.172 | 1.048 | 1.043 | 1.221 | 1.249 | 1.047 | 1.045 |
| O3″−H3′ | 1.751 | 1.726 | 1.995 | 1.988 | 1.692 | 1.637 | 2.010 | 1.981 |
| O3″−H2″ | 1.444 | 1.413 | 1.284 | 1.249 | 1.470 | 1.472 | 1.272 | 1.249 |
| O1″−H1″ | | | | | 1.001 | 0.998 | 0.980 | 0.972 |
| O2″−H2″ | 1.080 | 1.083 | 1.158 | 1.162 | 1.068 | 1.057 | 1.166 | 1.159 |
| O3″−H3″ | 1.184 | 1.201 | 1.126 | 1.131 | 1.246 | 1.265 | 1.143 | 1.154 |
| O1−Al−O2 | 100.1 | 100.3 | 100.0 | 100.3 | 99.3 | 99.5 | 97.1 | 97.3 |
| O2−Al−O3 | 102.7 | 103.3 | 99.0 | 100.2 | 101.5 | 101.9 | 100.5 | 101.1 |
| O3−Al−O1 | 86.5 | 87.5 | 83.6 | 84.1 | 93.2 | 95.3 | 89.1 | 89.9 |
| Al−H3″−O3″ | 155.7 | 155.3 | 160.4 | 160.2 | 149.0 | 148.6 | 157.2 | 156.3 |

50 kcal/mol lower in energy than the corresponding $Al^+(H_2O)_n$ for $n$ around 8. The reaction barrier is estimated to be around 10 kcal/mol for $n \geq 8$. There is no reason to believe that this value would increase significantly for larger $n$. In fact, reaction 2 is also observed in our AIMD simulations for $Al^+(H_2O)_{12}$ and $Al^+(H_2O)_{14}$ within 1 ps. Finally, the $H_2$ elimination reaction 1, observed around $n \geq 11$ for $Al^+(H_2O)_n$, should be due to the $HAlOH^+(H_2O)_{n-1}$ clusters, as they are the dominant isomers at these sizes, and the size-dependence effect of this reaction is determined by the structure and solvation dynamics of $HAlOH^+(H_2O)_{n-1}$.

***Table 6.*** Energy Barrier (kcal/mol) of the Insertion Reaction for $n = 8$ and 9[a]

| | 8-5 | | 9-4 | |
|---|---|---|---|---|
| level of theory | 6-31G* | 6-31G** | 6-31G* | 6-31G** |
| BPW91 | 4.6 | 4.3 | 7.6 | 7.2 |
| | (0.4) | (0.1) | (2.4) | (1.9) |
| MP2 | 12.2 | 11.7 | 15.7 | 15.0 |
| | (7.7) | (7.1) | (10.8) | (10.0) |

[a]The energies in the parentheses include zero-point correction.

**The Structures of $HAlOH^+(H_2O)_{n-1}$, $n = 6-9$.** Figures 10 and 11 show the structures of $HAlOH^+(H_2O)_{n-1}$, for $n = 6-14$.

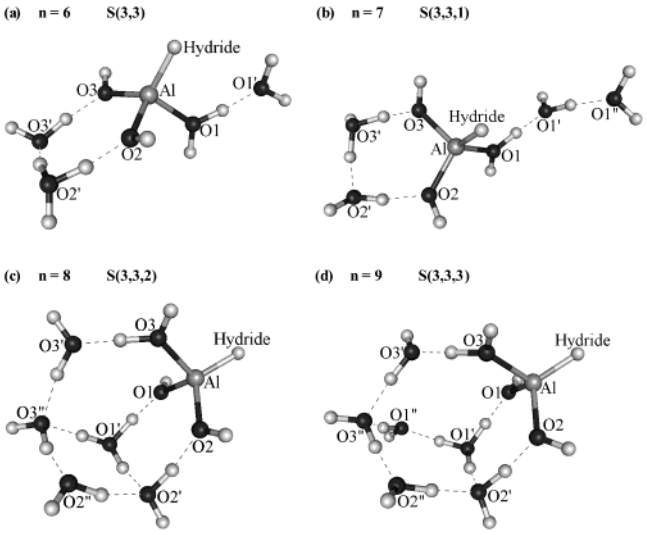


***Figure 10.*** Structures of $HAlOH^+(H_2O)_{n-1}$, $n = 6-9$. These are snapshot structures at the end of AIMD simulations at 300 K for these clusters. Water molecules aggregate on the opposite side of the Al−H bond.

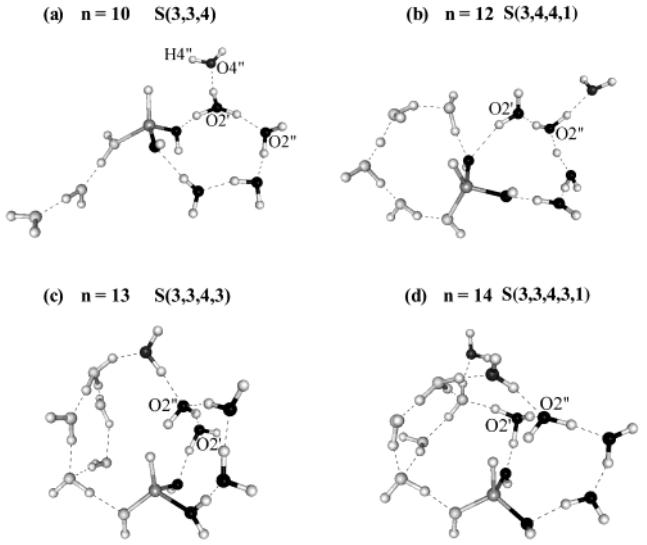


***Figure 11.*** Structures of $HAlOH^+(H_2O)_{n-1}$, $n = 10-14$. These are snapshot structures at the end of AIMD simulations at 300 K for these clusters. There are two wings around the Al−H bond, one colored gray and the other colored black. At $n = 13$, these two wings are connected over the top of the Al−H bond. Such cagelike structures provide the hydrogen bond $H_2O$ network along which a proton could be transferred to the vicinity of the Al−H bond. It makes the $H_2$ elimination reaction possible.

These structures are first obtained for $n = 8$ and 9, during the 3 ps AIMD simulation for $Al^+(H_2O)_n$, when $HAlOH^+(H_2O)_{n-1}$ is formed as the product of reaction 2. As shown in Figure 7 for $n = 9$, the six-water-ring and the three-water-tail both are tilted to the Al−H side of the cluster right after the reaction. As the simulation continues, these two structural features bend away from the Al−H bond. A further 3 ps AIMD simulation at 300 K is performed to see the stability of $HAlOH^+(H_2O)_{n-1}$ and to explore the possibility of $H_2$ elimination. Initial structures of $HAlOH^+(H_2O)_{n-1}$ of different sizes are formed either by removing $H_2O$ molecules successively, starting from $HAlOH^+(H_2O)_7$ ($n = 8$), or by adding successive $H_2O$ molecules on, starting from $HAlOH^+(H_2O)_8$ ($n = 9$). After a 500 time step equilibration run at 300 K, a 3 ps AIMD simulation at the same temperature is performed for each cluster. All of the structures

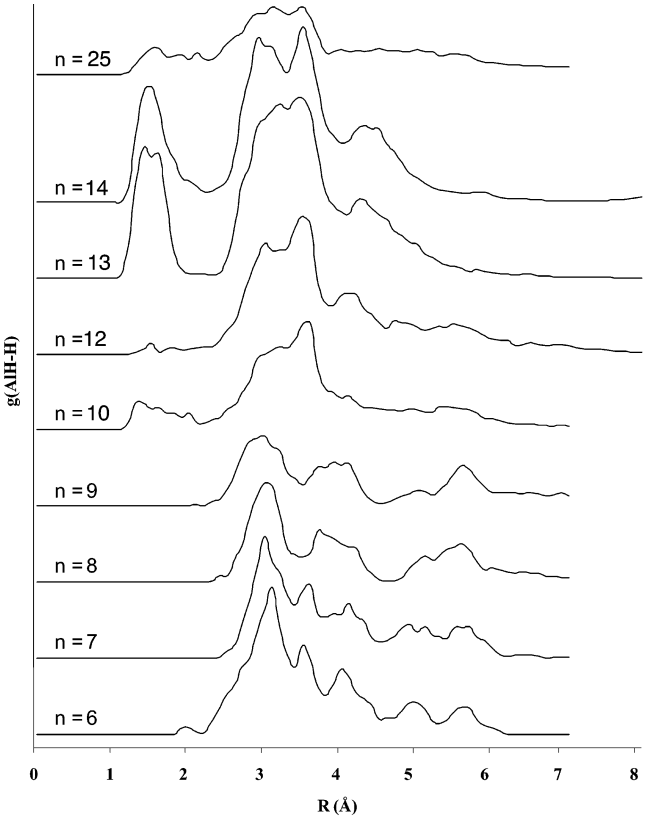


***Figure 12.*** Radial distribution function of H atoms around the hydride H in Al−H. A hydrogen peak is first observed at $n = 10$, indicating the presence of a proton near the Al−H bond. At $n = 13$ and 14, it becomes a well-defined peak with significantly enhanced intensity, indicating the increased probability of finding a proton near Al−H. At $n \approx 25$, this peak becomes weak and broadened, probably because of the diffusion of a proton through the growing $H_2O$ cage structure.

shown in Figures 10 and 11 are snapshots near the end of these simulations.

As compared to $Al^+(H_2O)_n$, the extent of acidic dissociation in $HAlOH^+(H_2O)_{n-1}$ is further intensified. This is clearly shown in Figure 8, with a significant increase in the fluctuation for the number of H around O atoms after reaction 2 takes place just below 2000 time steps. The $Al^{3+}$ in the $HAlOH^+(H_2O)_n$ clusters remains tetrahedrally coordinated, with hydride H on one side and three O atoms on the other. Such a structure is different from $Al^{3+}(H_2O)_n$ clusters, which were found to be octahedrally coordinated in a recent AIMD study, also using the planewave and pseudopotential based DFT method.[4]

The structures of $HAlOH^+(H_2O)_{n-1}$ show rich variation as $n$ changes. For $n = 8$, the six-water-ring is preserved and strengthened as shown in Figure 6, with a slight decrease in the fluctuation of hydrogen bond distance after the reaction. (Strictly speaking, it is no longer a six-water-ring, as one of the $H_2O$ is now a hydroxy group OH after reaction 2. Nonetheless, because of the constant shuffling of proton among $H_2O$ molecules, it is hard to pinpoint the hydroxy group. We retain the term "six-water-ring" for the sake of discussion and consistence.) Interestingly, the chain of two $H_2O$ molecules outside the six-water-ring in the $Al^+(H_2O)_8$ cluster **8-5** is now embedded into the six-water-ring, with the end $H_2O$ of the chain located at the center of the ring and taking the character of a hydronium ion $H^+{}_3O$ (Figure 10). For $n = 9$ ($HAlOH^+(H_2O)_8$), this basic feature is retained, and the added $H_2O$ is attached

***Table 7.*** Some Geometrical Distances (Å) of the Stable and Transition Structures and the Reaction Barrier (kcal/mol) for the $H_2$ Elimination Reaction at $n = 8$, 12, and 13[a]

| | $n = 8$ | | | | $n = 12$ | | | | $n = 13$ | | | |
|---|---|---|---|---|---|---|---|---|---|---|---|---|
| | stable structure | | transition structure | | stable structure | | transition structure | | stable structure | | transition structure | |
| | HF 6-31G** | MP2 6-31G** | HF 6-31G** | MP2 6-31G** | HF 6-31G** | MP2 6-31G** | HF 6-31G** | MP2 6-31G** | HF 6-31G** | MP2 6-31G** | HF 6-31G** | MP2 6-31G** |
| Al−O1 | 1.908 | 1.893 | 1.788 | 1.814 | 1.773 | 1.870 | 1.720 | 1.735 | 1.901 | 1.890 | 1.728 | 1.749 |
| O1−H1 | 0.946 | 0.964 | 1.261 | 1.283 | 1.639 | 1.081 | 1.921 | 1.825 | 0.985 | 1.046 | 1.880 | 1.770 |
| O1′−H1 | | | | | 0.980 | 1.348 | 0.953 | 0.974 | 1.598 | 1.431 | 0.955 | 0.980 |
| O1′−H1′ | | | | | 1.384 | 1.008 | 1.861 | 1.772 | 0.958 | 0.991 | 1.791 | 1.652 |
| O1″−H1′ | | | | | 1.047 | 1.572 | 0.956 | 0.980 | 1.836 | 1.669 | 0.960 | 0.993 |
| O1″−H1″ | | | | | 1.021 | 0.987 | 1.722 | 1.682 | 0.949 | 0.975 | 1.614 | 1.484 |
| O2″−H1″ | | | | | 1.458 | 1.701 | 0.969 | 0.992 | 2.046 | 1.860 | 0.984 | 1.033 |
| O2″−H2″ | | | | | 0.952 | 0.964 | 1.333 | 1.515 | 0.949 | 0.972 | 1.222 | 1.292 |
| H1−hydride | 3.093 | 3.160 | 1.018 | 1.014 | | | | | | | | |
| H2″−hydride | | | | | 1.915 | 2.318 | 0.896 | 0.821 | 1.985 | 1.861 | 0.976 | 0.926 |
| Al−hydride | 1.570 | 1.565 | 1.758 | 1.739 | 1.613 | 1.576 | 1.721 | 1.769 | 1.591 | 1.589 | 1.711 | 1.706 |
| relative energy | 0.0 | 0.0 | 42.9 | 32.6 | 0.0 | 0.0 | 7.9 | 11.9 | 0.0 | 0.0 | 21.7 | 11.7 |

[a] The basis set is 6-31G**. Energies include zero-point energy correction evaluated by HF harmonic frequencies calculations at the HF optimized geometries.

right to the end of the hydronium ion in $HAlOH^+(H_2O)_7$. There are also changes in the connections of the hydrogen bonded rings (Figure 10).

When $n$ is decreased to 6 and 7 ($HAlOH^+(H_2O)_5$ and $HAlOH^+(H_2O)_6$), the six-water-ring is disrupted. In its place, there is a four-water-ring, with the other $H_2O$ molecules forming a chain. It is obvious from an examination of these structures that the $H_2$ elimination is difficult for $HAlOH^+(H_2O)_{n-1}$ clusters of the size $n = 6-9$. The Al−H bond is polar with H as the negative end,[30] but its polarity is much less than that for the O−H bond in $H_2O$ molecules. As a result, the $H_2O$ molecules will aggregate among themselves, leaving the Al−H bond alone on the surface of the cluster, and away from other hydrogen atoms (and $H^+$). Thus, $H_2$ formation cannot happen. Similar structural features have been observed before in the hydrated halide anion clusters, such as $Cl^-(H_2O)_n$ and $Br^-(H_2O)_n$,[68] and hydrated metal atom clusters, such as $Na(H_2O)_n$,[69] in which the halide anion or the metal atom would also stay on the surface of the cluster. As the water−water interaction is stronger than the water−anion or water−metal interaction, the water molecules would prefer to aggregate among themselves.

**The Structures of $HAlOH^+(H_2O)_{n-1}$, $n = 10-14$.** For the $H_2$ elimination to take place, a proton should be combined with the hydride H in Al−H to produce $H_2$. As discussed above, acidic dissociation is quite extensive within $HAlOH^+(H_2O)_{n-1}$, and protons are available. The deciding factor is then that the solvent $H_2O$ molecules have to be arranged in a way so that a proton could be transferred through the hydrogen bonded $H_2O$ network and brought near Al−H.

The evolution of $HAlOH^+(H_2O)_{n-1}$ structures, $n = 10-14$, shown in Figure 11, satisfies this requirement. Going from $n = 9$ to $n = 10$, the six-water-ring is preserved with an additional $H_2O$ connected to the $H_2O$ at O2′, and a linear chain of three $H_2O$ molecules disengages itself from the six-water-ring. As more $H_2O$ molecules are added, this chain starts to curl up at $n = 12$ to form yet another six-water-ring structure. The two rings are like two wings, approximately sitting in a plane perpendicular to the Al−H bond. On the old six-water-ring, the extra $H_2O$ now moves to the O2″ position. At $n = 13$, the new ring transforms itself into a five-water-ring structure that does not involve any first shell $H_2O$. Meanwhile, both the six-water-ring and the five-water-ring are bent further up over the Al−H bond and are linked by the $H_2O$ molecule attached to O2″ on the six-water-ring. This linkage indicates a remarkable transition in the $HAlOH^+(H_2O)_{n-1}$ structure, from the small ($n \leq 9$) cluster structure with the Al−H bond on the cluster surface and pointed away from all the other $H_2O$ molecules, to a caged structure with the Al−H buried inside. Because of the polarity of the Al−H bond with H being the slightly negative end,[30] the hydride could now attract protons to its vicinity through the hydrogen bond $H_2O$ network. At $n = 14$, one more link is added between the five- and six-water-rings, and these two links are themselves a part of a new five-water-ring. This kind of five-water-rings has been reported before in large hydrated proton clusters $H^+(H_2O)_n$.[50]

The change in structure is also reflected in the radial distribution function of H atoms around the hydride H, as shown in Figure 12, obtained from AIMD simulations at 300 K. For $HAlOH^+(H_2O)_{n-1}$, $n = 6-9$, all hydrogen atoms are more than 2 Å away from the hydride H, indicating that $H_2$ formation should be quite unlikely for these clusters. For $HAlOH^+(H_2O)_{n-1}$, $n = 10$ and 12, the presence of H atoms between 1 and 2 Å away from the hydride H is seen, albeit the peak is weak and broad. For $HAlOH^+(H_2O)_{n-1}$, $n = 13$ and 14, the cage structure over the Al−H bond brings protons near the hydride, and there appears a well-defined strong peak centered around 1.5 Å. One would thus expect a significant increase in the probability for the formation of $H_2$ between the hydride H and one of the protons around it.

Experimentally, $H_2$ elimination was observed starting at the mass of $Al^+(H_2O)_{11}$, which was equivalent to the isomer $HAlOH^+(H_2O)_{10}$. The reaction rate then jumped up at $n = 13$, but fell back at $n = 14$. Another big increase was observed at $n = 17$ and beyond, until it decreased around $n = 22-24$ and finally dropped to zero beyond $n = 25$.[23,24] The observed structural changes in $HAlOH^+(H_2O)_{n-1}$ are consistent with the pattern around the onset of reaction 1 and especially with the significant rate increase at $n = 13$.

**Reaction Barriers for $H_2$ Elimination in $HAlOH^+(H_2O)_{n-1}$.** Two independent approaches were used to estimate the barrier

(68) Combariza, J. E.; Kestner, N. R. *J. Chem. Phys.* **1994**, *100*, 2851.
(69) Hashimoto, K.; Morokuma, K. *J. Am. Chem. Soc.* **1994**, *116*, 11436.

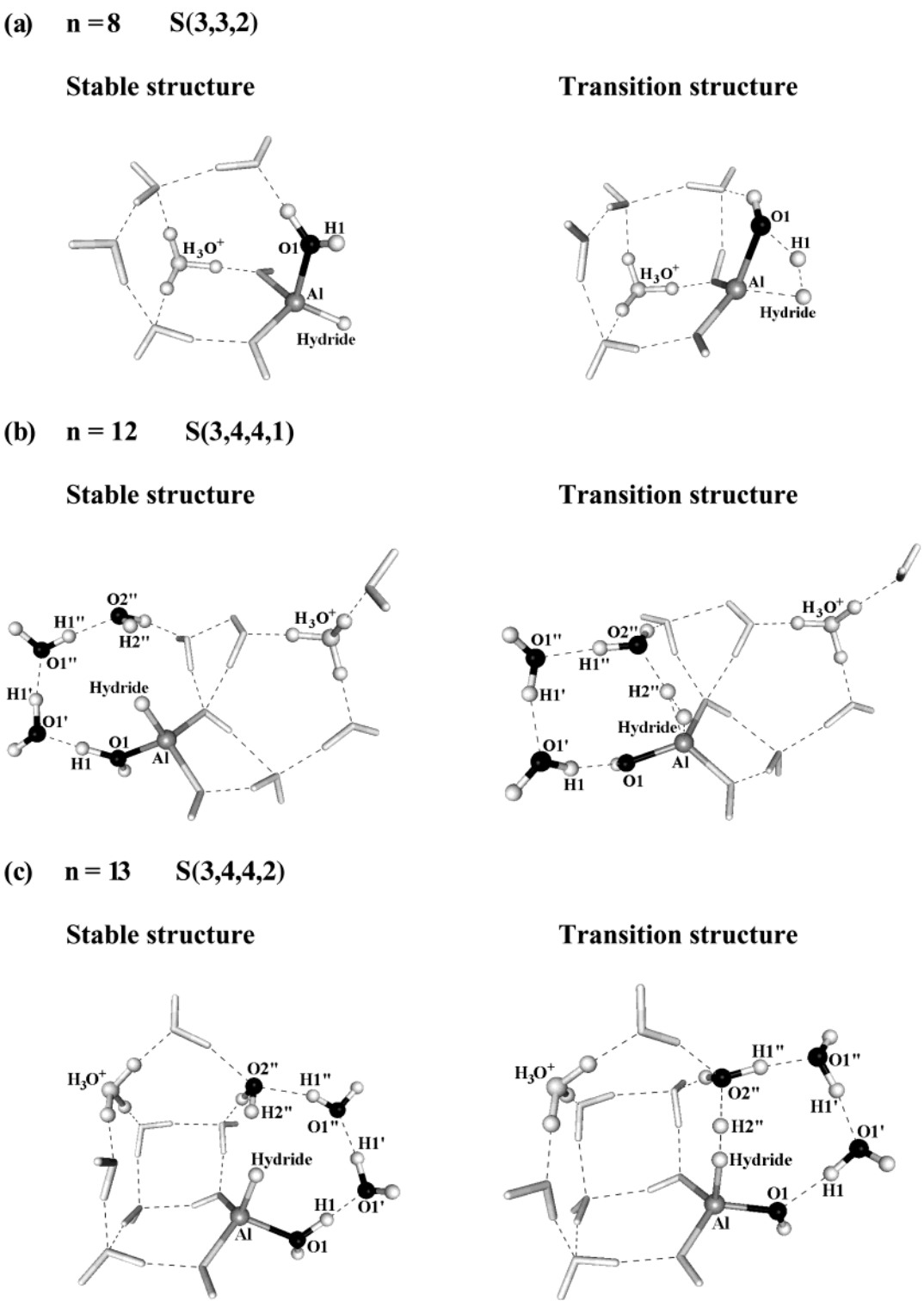


***Figure 13.*** Transition structures obtained at the MP2/6-31G** level for the intracluster $H_2$ loss reaction in $HAlOH^+(H_2O)_{n-1}$, $n = 8$, 12, and 13, as well as the corresponding stable $HAlOH^+(H_2O)_{n-1}$ structures. Notice the H attacking the hydride comes from the first solvation shell for $n = 8$, in contrast to $n = 12$ and 13, for which the attacking H comes from the third solvation shell. As a result, the energy barrier for $n = 8$ is much higher.

for the $H_2$ elimination. In the first approach, the Hartree−Fock method at the 6-31G** and MP2/6-31G** levels was directly applied to search for the transition structures. For $n = 12$ and 13, the hydrogen atom attacking the hydride came from the third solvation shell. The energy barrier, with zero-point energy correction included, was found to be 11.9 kcal/mol for $n = 12$, and 11.7 kcal/mol for $n = 13$, at the MP2/6-31G** level. In contrast, the barrier for $n = 8$ was found to be much higher at a value of 32.6 kcal/mol, shown in Table 7. As discussed in the previous section, the water molecules aggregate among themselves on the opposite of the Al−H bond for $n = 8$, and the attacking H had to come from a water molecule in the first solvation shell. The transition structure for $n = 8$, shown in Figure 13, contains a highly strained four-member H−Al−O1−H1 ring. Such structural features result in a much higher barrier for $H_2$ formation for $n = 8$.

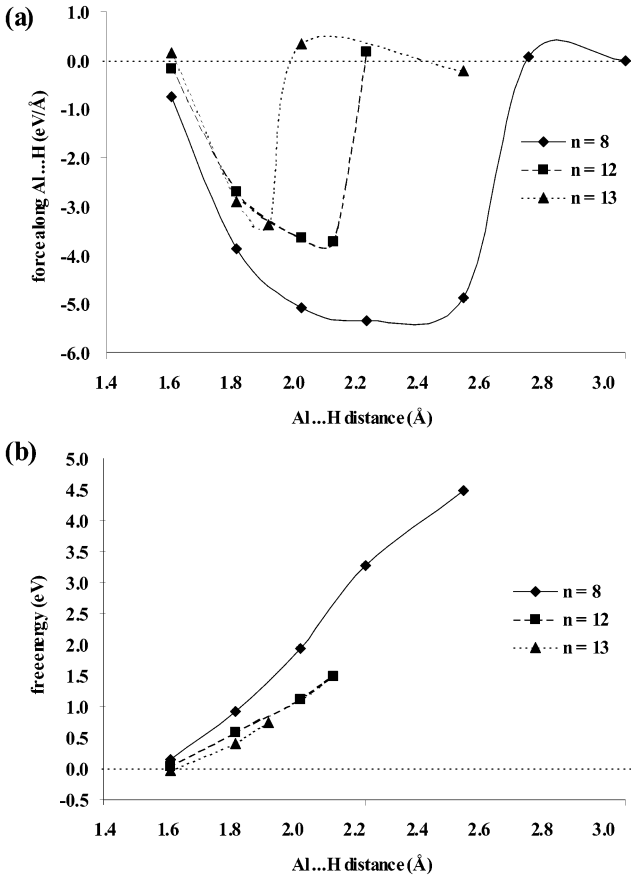


***Figure 14.*** Average forces along the Al−H bond, obtained from the AIMD simulations for $n = 8$, 12, and 13, at 300 K, with the Al−H distance constrained. The negative value of the force indicates resistance to the stretching of the Al−H bond. When the $H_2$ is formed, the value of the average force drops to zero. Integration over the force curve gives the free energy barrier for the $H_2$ elimination.

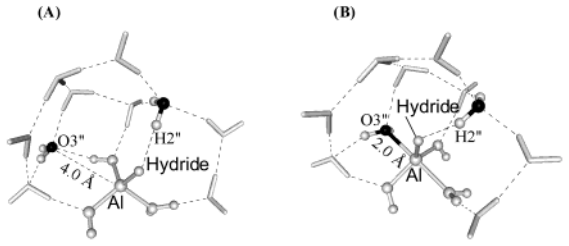


| Al-O distance (Å) | Relative energy (kcal/mol) | | | |
|---|---|---|---|---|
| | HF/6-31G** | | MP2/6-31G**//HF/6-31G** | |
| | without BSSE | with BSSE | without BSSE | with BSSE |
| 4.0 | 0.0 | 0.0 | 0.0 | 0.0 |
| 3.5 | 1.3 | 1.4 | | |
| 3.0 | 2.5 | 2.7 | 3.3 | 3.4 |
| 2.5 | 3.7 | 4.7 | | |
| 2.0 | 6.5 | 8.9 | 4.5 | 9.0 |

***Figure 15.*** Optimized structures for $HAlOH^+(H_2O)_{n-1}$, $n = 13$, with the O3″−Al distance contrainted at 4.0 Å for **A** and 2.0 Å for **B**, in a nucleophilic attack on the $Al^{3+}$ by the $H_2O$ molecule at O3″. The table shows that the relative energy increases as the O3″−Al distance decreases, and, when no constraint is applied, **B** goes back to **A** during optimization.

For $n = 10$, the presence of a water molecule attached to the six-water-ring (labeled as O4″ in Figure 11) provides an alternative reaction path, with H4″ attacking the H−Al bond. However, we failed to locate a transition structure for such a process, as the O4″ water molecule dissociated away during optimization. This observation could be attributed to the fact that the O4″ water molecule is not part of the six-water-ring, and the acidic dissociation along the H4″−O4″ bond should be considerably less in extent than that in the six-water-ring. Thus, for $H_2$ elimination in $HAlOH^+(H_2O)_{n-1}$, $n = 10$, the attacking H should again come from the first solvation shell, as in the case for $n = 8$, and the reaction barrier should be quite high. These results indicate the onset of the intracluster $H_2$ elimination for $n > 10$, in good agreement with experiments.[23,24]

Because the clusters are of considerable sizes and bounded together by the relatively weak hydrogen bonds, there must be a number of local structures and first order saddle points. A slight change in the computational method could lead to a different local minimum and to considerable changes in the value of the barrier. Mapping out all these local and transition structures would be quite a challenge. Moreover, the approach assumes that these structures are static, while in reality these clusters are floppy at constant temperature. The barrier values should thus only be taken as an indication of whether the hydrogen loss reaction is energetically accessible.

We attempted to address this problem in our second approach, in a set of AIMD simulations at 300 K for $n = 8$, 12, and 13, respectively, with the hydride Al−H distance treated as the reaction coordinate and constrained by RATTLE method.[70] At each constrained value, the force along the Al−H bond is averaged from a simulation of 7500 time steps (3 ps). In this way, the phase space is sampled and averaged so that the dynamic and entropic factors can be accounted for. As shown in Figure 14, a negative force indicates that the force is against the stretching of the Al−H bond, and the sudden increase of the force to just above zero coincides with the formation of $H_2$. As expected, the resisting force for $n = 8$ is much larger than that for $n = 12$ or $n = 13$. Integrating over the force curve versus Al−H distance gives us a rough estimate of the free energy barrier for the $H_2$ elimination reaction. The barrier is 0.7 eV (16 kcal/mol) for $n = 13$, 1.5 eV (35 kcal/mol) for $n = 12$, and 4.5 eV (100 kcal/mol) for $n = 8$.

We cannot directly compare the barriers obtained by these two approaches, as the MP2/6-31G** results are energy barriers, while the AIMD results are free energy barriers. Although the AIMD method almost certainly overestimates the strength of hydrogen bonds and the extent of acidic dissociation, it provides a much better account for the solvation dynamics and the entropy factor. The size-dependence effect is much more prominent in the AIMD estimate, characterized by the rapid change of the reaction barrier with varying $n$, than that in the MP2/6-31G** calculations. However, both approaches identified a trend of change in the barriers that is consistent with the experimentally observed switch-on of the $H_2$ elimination and the structural changes for $HAlOH^+(H_2O)_{n-1}$ clusters with increasing $n$.

It is interesting to notice that although the AIMD free energy barrier for the elimination reaction 1 at 16 kcal/mol (for $n = 13$) is not very high, we did not observe it in any of our constraint-free AIMD simulations of $HAlOH^+(H_2O)_{n-1}$ at

(70) Anderson, H. C. *J. Comput. Phys.* **1983**, *52*, 24.

300 K. Heating up to higher temperature was attempted for $HAlOH^+(H_2O)_{12}$ ($n = 13$), but only resulted in the evaporation of $H_2O$ molecules. This is in contrast to the isomerization reaction 2, which is easily observed in all of our simulations for $Al^+(H_2O)_n$, with $n \geq 8$.

The difference could be attributed qualitatively to the entropy factor. For reaction 2, the stability and presence of the six-water-ring structure fixes a hydrogen (H3″ in Figure 9) pointing right at the $Al^+$, and the probability for seeing the reaction is almost assured, while for the hydrogen elimination reaction in $HAlOH^+(H_2O)_{n-1}$, the protons produced in acidic dissociation could be distributed all over the hydrogen bonded $H_2O$ network, and there is no comparable restraining structural features to fix a proton near the Al−H bond. As a result, the probability of seeing an $H_2$ elimination reaction in our simulations is much reduced, and our simulation time of 3 ps is probably not long enough. Experimentally, the rate of the hydrogen elimination for $Al^+(H_2O)_n$ was observed within a period of a few seconds.[23]

**Nucleophilic Attack on $Al^{3+}$ Ion in $HAlOH^+(H_2O)_{n-1}$.** For $Al^{3+}$, the coordination number should be either 4 or 6,[47] in contrast to the $Al^+$ in $Al^+(H_2O)_n$, for which the coordination number is 3. The $HAlOH^+(H_2O)_{n-1}$ isomers in our report are formed by the insertion process from $Al^+(H_2O)_n$, and the coordination number around the Al ion is 4, with three oxygen atoms and one $H^-$ from the hydride bond. There is the interesting possibility of nucleophilic attacks on the $Al^{3+}$ from $H_2O$ molecules within the cluster. Furthermore, such processes could also be coupled with the $H_2$ elimination.

We examined these possibilities for $HAlOH^+(H_2O)_{n-1}$, $n = 13$. Because of its geometry, the most likely path for a nucleophilic attack is from O3″, a $H_2O$ molecule in the third shell, as shown in Figure 15. Such an attack would change the coordination number around $Al^{3+}$ from 4 to 5, as an intermediate step to change the coordination number eventually to 6. For the HF/6-31G** optimized structure, the O3″−Al distance is around 4.0 Å, in contrast to the first shell O−Al distance around 2.0 Å. Structural optimization is performed with the O3″−Al distance contrained to a constant value. As the distance is gradually decreased from 4.0 to 2.0 Å, the hydrogen bond network is not disrupted, while the total energy at the MP2/6-31G**//HF/6-31G** level increases by 4.5 kcal/mol, and by 9.0 kcal/mol when basis set superposition error (BSSE) is considered. BSSE correction becomes more important as the O3″−Al distance decreases, due to the change in coordination number. The energy difference of 9.0 kcal/mol is not very large for an ionic cluster $HAlOH^+(H_2O)_{n-1}$, with $n = 13$. However, once the constraint on the O3″−Al distance is released in a full structure optimization, **B** in Figure 15 goes back to **A**, which indicates that such a nucleophilic attack does not lead to a stable intermediate structure.

Starting with **B**, we also attempted to search for a transition structure, by considering the attack of H2″ on the hydride H. This is a mechanism in which the formation of $H_2$ is concerted with a nucleophilic attack. No transition structure was found, and the optimization always led back to **A**. These results could probably be attributed to the presence of the hydride Al−H bond in $HAlOH^+(H_2O)_{n-1}$. The Al−H distance around 1.6 Å is significantly lower than the Al−O distance (see Table 7), and the hydride H has a large steric effect blocking nucleophilic attacks from other $H_2O$ molecules.

No nucleophilic attack was observed during the AIMD simulation. As the Al−H distance increases in the constraint AIMD simulations, an $Al(OH)_2(H_2O)^+$ ion core is formed with a roughly planar structure, and nucleophilic attack by other water molecules could theoretically take place from the two sides of the planar ion core. Yet with the Al−H bond pointed into the water cluster, the constrained H atom blocks the inner side of the $Al(OH)_2(H_2O)^+$ ion core, and thus water molecules could not attack from this side. On the other hand, the Al ion is situated on the surface of the cluster, and there is no water molecule at the outer side of the planar ion core.

Nonetheless, in an additional MD run with the Al−H constraint removed after the formation of a $H_2$ molecule, the $H_2$ molecule went away, and, afterward, the trigonal planar isomer was unstable, and a tetrahedral ion core, $Al(OH)_2^+(H_2O)_2$, was formed within hundreds of time steps (500 fs).

**The Switch-Off of the $H_2$ Elimination for $n > 24$.** The switch-off of the $H_2$ elimination in $Al^+(H_2O)_n$ clusters occurs for $n > 24$,[23,24] and unfortunately simulations on $HAlOH^+(H_2O)_{n-1}$ around such a size are very expensive, because the volume of the periodic cell must be increased to accommodate the spatial extent of the cluster ion. As an approximation, we performed a 3 ps simulation at 300 K on $Al^+(H_2O)_{25}$, using a periodic cubic box with a length of only 14 Å. Obviously, there are interactions between $H_2O$ molecules in the neighboring cells, and $n = 25$ is not an accurate indication of the cluster size. However, such interactions on the outside region of the cluster can be taken averagely as the presence of additional solvent $H_2O$ molecules, and the system is approximately treated as an $Al^+(H_2O)_n$ cluster with $n$ being ill defined, but certainly larger than 25.

Starting from $Al^+(H_2O)_{25}$, the cluster went through the insertion reaction 2 spontaneously within a few hundred time steps. It indicates that the insertion process is not adversely affected by the increasing cluster size, and the switch-off should be an effect on the elimination reaction only. At first look, the structure of the newly formed $HAlOH^+(H_2O)_{24}$ is not much different from $HAlOH^+(H_2O)_{n-1}$ for $n = 13$ and 14 (Figure 11). The $Al^+$ with its immediate first shell ligands is on the surface of the cluster, while the outer layer $H_2O$ molecules form a cage structure, and the Al−H bond is buried inside the cage. However, a closer look at the radial distribution of H around the hydride Al−H reveals a difference; the first hydrogen peak around 1.5 Å becomes flat and broadened, as shown in Figure 12, in contrast to the sharp and well-defined first H peak for $n = 13$ and 14.

A detailed understanding of the structural change leading to the flattening of the first hydrogen peak will have to wait for more elaborate simulations on clusters of the size around $n = 24$. However, our preliminary result does hint a new mechanism for the switch-off of the elimination reaction 1. For $n = 13$ and 14, the presence of the 1.5 Å hydrogen peak in Figure 12 is due to the protons brought into the vicinity of the Al−H bond by the $H_2O$ cage structure. As the $HAlOH^+(H_2O)_{n-1}$ cluster increases in size, the cage grows accordingly. There is thus an increasing probability for the protons produced in the acidic dissociation to diffuse through the extended cage, and accordingly the first hydrogen peak becomes lowered and broadened for $n \approx 25$. After all, the hydride H is not as negatively charged as the O atom in the water molecules. As a result, the hydride

Al−H is deprived of the proton needed for the elimination reaction, and the consequent significant drop in reaction rate thus contributes to the experimentally observed switch-off of the hydrogen elimination reaction.

## Summary

New insights into the structure, dynamics, and reactivities of $Al^+(H_2O)_n$ clusters were revealed from AIMD simulations, in combination with the Gaussian based Hartree−Fock/MP2 and DFT methods, and the mechanism for the intracluster $H_2$ elimination was explored.

It was found that for small clusters $Al^+(H_2O)_n$, $n = 6-9$, structures with a six-water-ring that involves 12 members, including $Al^+$ and $H_2O$ molecules from the first, second, and third shells, are favored. The existence of such structures is verified by Gaussian based DFT/BPW91 and HF/MP2 calculations with 6-31G* and 6-31G** basis sets. The prominent features of this six-water-ring are its stability, enhancement of acidic dissociation, and, most importantly, use as a precursor to the insertion reaction producing $HAlOH^+(H_2O)_{n-1}$, for $n \geq 8$. The reaction barrier is at 10.0 kcal/mol for $n = 9$ and 7.1 kcal/mol for $n = 8$, at the MP2/6-31G** level. As a result, the experimentally observed $H_2$ elimination reactions for $n = 11-24$ are due to the $HAlOH^+(H_2O)_{n-1}$ clusters, rather than $Al^+(H_2O)_n$.

For small $HAlOH^+(H_2O)_{n-1}$ clusters with $n = 6-9$, our studies show that the Al−H bond is at the cluster surface, pointing away from all of the other $H_2O$ molecules, and $H_2$ formation is impossible. However, the cluster structure changes as $n$ increases, and, at $n = 13$, a cage structure is formed that wraps the Al−H bond inside the cage. This trend could explain the switch-on of the $H_2$ elimination reaction, as the cage delivers protons to the regions near Al−H bond. Constrained dynamics simulations estimate the free energy barrier for $H_2$ elimination to be 0.7 eV (16 kcal/mol) for $n = 13$, 1.5 eV (35 kcal/mol) for $n = 12$, and 4.5 eV (100 kcal/mol) for $n = 8$. Transition structures for this reaction have also been identified at the MP2/6-31G** level for $n = 8$, 12, and 13.

For $Al^+(H_2O)_n$ with $n > 25$, our preliminary simulation shows that the insertion reaction again takes place spontaneously and is not affected by the increasing size of $HAlOH^+(H_2O)_{n-1}$. On the other hand, the $H_2$ elimination reaction in $HAlOH^+(H_2O)_{n-1}$ does become much more difficult, as protons produced in the acidic dissociation diffuse through the extended $H_2O$ network and leave the vicinity of the Al−H bond.

**Acknowledgment.** Computations reported in this paper were performed on the AlphaStation clusters operated by the Department of Chemistry, the Chinese University of Hong Kong (CUHK), supported by a Special Equipment Grant, and on the SGI Origin 2000, at the Steacie Institute for Molecular Sciences, National Research Council of Canada. We thank Mr. Ka Fai Woo at the Department of Chemistry and Mr. Frank Ng at the Information Technology Services Center, both of CUHK, for technical support. We gratefully acknowledge the financial support provided by the Research Grant Council, Hong Kong SAR Government, through Project CUHK 4276/00P.

**Supporting Information Available:** Cartesian coordinates for all of the structures shown in Figures 1−5, 7, 9−11, and 13 (PDF). This material is available free of charge via the Internet at http://pubs.acs.org.

JA0117579